Cement and Concrete Research 142 (2021) 106370

Contents lists available at ScienceDirect

Cement and Concrete Research

journal homepage: www.elsevier.com/locate/cemconres

Effect of temperature curing on properties and hydration of wollastonite blended magnesium potassium phosphate cements

Biwan Xu [a,b], Frank Winnefeld [a], Barbara Lothenbach [a,c,*]

[a] Laboratory for Concrete & Construction Chemistry, Swiss Federal Laboratories for Materials Science and Technology (Empa), 8600 Dübendorf, Switzerland
[b] CEA, DES, ISEC, DE2D, Univ Montpellier, Marcoule, France
[c] Department of Structural Engineering, Norwegian University of Science and Technology, Trondheim, Norway

ARTICLE INFO

Keywords:
Magnesium potassium phosphate cement
Wollastonite
Temperature curing
Hydration
Thermodynamic modelling

ABSTRACT

K-struvite, the main hydrate of magnesium potassium phosphate (MKP) cements, dehydrates at ~50 °C, thus elevated temperatures at service conditions could affect cement properties and durability. In this study, properties and hydration of MKP cement without and with wollastonite were investigated at 20 and 50 °C. In hydrated pure MKP cement K-struvite decomposes progressively over time to $MgKPO_4{\cdot}H_2O$ at 50 °C, which leads to a strong reduction of solid volume and severe strength loss. The presence of wollastonite significantly slows down the decomposition rate of K-struvite, which is still observed after 393 days at 50 °C. K-struvite together with amorphous hydroxyapatite, M-(C)-S-H and $CaK_3H(PO_4)_2$ from the wollastonite reaction result in a cement with good short and long-term strength at both 20 and 50 °C.

1. Introduction

Magnesium potassium phosphate (MKP) cements harden through an acid-base reaction between hard- or dead-burnt magnesia and potassium monophosphate (KH_2PO_4). The predominant hardening mechanism of MKP cements involves a dissolution-precipitation process and can be described by the following equation:

$$MgO + KH_2PO_4 + 5H_2O \rightarrow MgKPO_4{\cdot}6H_2O\ (K-struvite) + Q_{heat} \quad (1)$$

As represented in Eq. (1), K-struvite is the stoichiometric reaction product of hydrated MKP cements and provides mechanical strength. MKP cements have a different hydration chemistry than Portland cements, show fast setting [1,2], rapid strength gain [3–6], strong bonding to concrete substrates [3,7,8], low pH [6,9–11], as well as the ability to immobilize heavy metals [12–14], and are biocompatible [15–17].

In addition to K-struvite, other magnesium (potassium) phosphate hydrates including phosphorrösslerite ($MgHPO_4{\cdot}7H_2O$), newberyite ($MgHPO_4{\cdot}3H_2O$), $Mg_2KH(PO_4)_2{\cdot}15H_2O$, $Mg_3(PO_4)_2{\cdot}4H_2O$, bobierrite ($Mg_3(PO_4)_2{\cdot}8H_2O$), cattiite ($Mg_2(PO_4)_3{\cdot}22H_2O$) and $MgKPO_4{\cdot}H_2O$ can precipitate as intermediate phases during the hydration or as final products, depending mainly on the magnesium-to-phosphate (Mg/PO_4) molar ratio and the water-to-binder (w/b) ratio used [6,9–11,18–21].

Temperature is another important factor affecting hydrate assemblages and properties of magnesium phosphate cements [22]. While little is known on the temperature behaviour of MKP cements, it has been found that magnesium ammonium phosphate cements, which use ammonium phosphates instead of KH_2PO_4, showed a dehydration of struvite ($NH_4MgPO_4{\cdot}6H_2O$) to dittmarite ($NH_4MgPO_4{\cdot}H_2O$) above 70 °C, leading to a significant strength loss [22]. Temperatures affected also the stability of synthesized magnesium (potassium) phosphate hydrates. An increase in temperature from 20 to 80 °C led to a destabilisation of cattiite to bobierrite or $Mg_3(PO_4)_2{\cdot}4H_2O$, and to a destabilisation of K-struvite to $MgKHPO_4{\cdot}H_2O$ [23]. Such changes at relatively low temperatures (~45–65 °C) of different magnesium (potassium) phosphate hydrates such as K-struvite, phosphorrösslerite, $Mg_2KH(PO_4)_2{\cdot}15H_2O$ and cattiite [6,9–11,18,23,24] raise concerns about the stability of MKP cements at service conditions with elevated temperatures.

The changes of properties and hydrate assemblages of pure MKP cements and MKP cements blended with mineral additions such as fly ash, slag, wollastonite under a short time exposure (e.g. 3 h) to 200–1000 °C have been reported previously [25–27], which offer valuable information on MKP cements in practical applications that are subjected to some very harsh conditions such as potential fire incidents

* Corresponding author at: Laboratory for Concrete & Construction Chemistry, Swiss Federal Laboratories for Materials Science and Technology (Empa), 8600 Dübendorf, Switzerland.
E-mail address: Barbara.lothenbach@empa.ch (B. Lothenbach).

https://doi.org/10.1016/j.cemconres.2021.106370
Received 17 September 2020; Received in revised form 23 November 2020; Accepted 11 January 2021
Available online 9 February 2021

[25]. However, studies of the long-term behaviour of MKP cements at slightly elevated temperatures, e.g. 50 °C, close to the onset of the dehydration temperature of K-struvite, are not available in the open literature.

Wollastonite can be used to replace a part of the MKP cement, to slow down cement hydration kinetics and to lower heat release [11]. Wollastonite ($CaSiO_3$) has little reaction at pH > 9, while it is very reactive at low pH values [28]; therefore, it has been used as a starting material for low pH cements, i.e. cements with a pH <12, such as brushite cements [29,30], carbonated wollastonite-based cements [31], and as a reactive filler in wollastonite blended MKP cements [11,26]. The reaction of wollastonite in MKP cements leads to the formation of amorphous hydroxyapatite and magnesium-(calcium)-silicate (M-(C)-S-H) hydrates and improved strengths at late ages [11]. In addition, wollastonite blended MKP cements were reported having a good heat resistance when subjected to temperatures ranging from 200 to 1000 °C for 3 h [26].

The aim of this study was to unravel the changes of properties and hydrate assemblages of pure and wollastonite blended MKP cements cured at 50 °C, which is close to the onset dehydration temperature of K-struvite [18,24]. For comparison, samples cured at ambient conditions (20 °C, 70% relative humidity) were examined as well. A moderate Mg/PO_4 molar ratio of 4 was used in this study due to the consideration of practical use in the civil engineering field [8,18,21], in contrast to our previous work on wollastonite blended MKP, where a low Mg/PO_4 molar ratio of 2.7 was used [11]. The hydrated MKP cement pastes were characterized by using various methods, and thermodynamic modelling, which has been applied successfully to various types of hydrated cements [32–35], was employed to calculate the thermodynamically stable hydrates formed in pure and wollastonite blended MKP cements in a temperature range of 5–100 °C.

2. Materials and methods

2.1. Materials

The starting materials included dead-burnt magnesia, wollastonite and KH_2PO_4. Table 1 gives the chemical composition of these materials as determined by X-ray florescence (XRF) analysis. The mineralogical composition of the magnesia and wollastonite was determined by X-ray diffraction (XRD, CoKα, PANalytical X'Pert Pro) and has been reported already in [11]. The magnesia contained mainly periclase (MgO) and minor amounts of forsterite (Mg_2SiO_4) and monticellite ($CaMgSiO_4$); while the wollastonite contained mainly wollastonite-2M ($CaSiO_3$) and traces of α-quartz (SiO_2) and calcite ($CaCO_3$).

The particle size distributions of the starting materials as determined by laser diffraction (Malvern Mastersizer X, dispersion in isopropanol) are displayed in Appendix A. The mean particle sizes (d_{50}) of the magnesia, wollastonite and KH_2PO_4 averaged from triplicate measurements are 19.0 ± 0.3, 3.7 ± 0.5, and 34.4 ± 4.8 μm, respectively.

Table 2 provides the paste mix designs used in this study. All pastes were prepared using a Mg/PO_4 molar ratio of 4 and a water-to-binder ratio (w/b) of 0.25. The binder includes magnesia, wollastonite and KH_2PO_4. The magnesia and wollastonite had equal contents in the wollastonite blended paste (P4-W). The final setting times of the pastes were also given in Table 2. To be able to investigate the effect of wollastonite on the hydration of properties of the MKP cements, retarders, like boron compounds, were not used in this study.

2.2. Methods

2.2.1. Volume stability

Based on the mix designs given in Table 2, the solid starting materials were pre-mixed first before water addition. The mixing of the pastes was carried out using a vacuum mixer at 250 rpm for 3 min. Prisms with the dimensions of 20 mm × 20 mm × 100 mm were cast and demoulded right after their final settings (Table 2). Aluminum gauge studs were glued to both ends of the prisms using an epoxy adhesive at 20 °C and relative humidity (R.H.) of 70%. The lengths of the prisms were measured with a micro-meter comparator (ABSOLUTE, Mitutoyo). The first reading was made 1 h after the water addition to dry mixture. Thereafter, the prepared prisms were divided into two groups and cured under different regimes:

- Prisms were cured at room temperature (20 °C) and R.H. 70%, which was denoted as "*RT*".
- Prisms were cured at 20 °C and R.H. 70% for 7 days first, and then stored in oven at 50 °C for specified ages, which was denoted as "*7d RT + xd 50 °C*". To avoid fast water evaporation at 50 °C, prisms were carefully wrapped with several layers of polypropylene film and with a final layer of aluminum foil.

Prism lengths were measured periodically, and the relative length changes with increasing ages were calculated.

2.2.2. Mechanical strength

Following same casting protocol as described above, prisms with the same dimensions of 20 mm × 20 mm × 100 mm were fabricated for strength measurement. The samples were divided into two groups, and the same curing regimes as described above were applied. A three-point bending test was conducted first using a loading rate of 20 N/s and a span of 60 mm. Two prisms were measured for each paste per sample age. Afterwards, the obtained four prism halves were used for compressive strength measurement at a loading rate of 1 MPa/s and a contact surface area of 20 mm × 20 mm.

2.2.3. X-ray diffraction analyses and thermogravimetry

The hydration of pastes was stopped following the protocol recommended in [36,37]. Small sample pieces were collected after the compression test and stored in isopropanol for about 15 min. Afterwards, isopropanol was removed by filtration under vacuum, and diethyl ether was used to rinse the remaining solids and removed subsequently by filtration as well. The obtained solids were then dried at 40 °C for about 10 min to remove any remaining organic solvents. After the hydration stoppage, the solids were ground by hand into powders with a grain size < 63 μm.

XRD analyses were performed with a PANalytical X'Pert Pro in a θ-θ configuration using CoKα radiation and the X'Celerator detector. The powder samples were scanned between 5° and 90° 2θ for 45 min.

Thermogravimetric (TGA) analyses were conducted from 30 to

Table 1
Chemical composition of the starting materials wt%.

Materials	MgO	SiO_2	Al_2O_3	Fe_2O_3	CaO	K_2O	Na_2O	TiO_2	SO_3	P_2O_5	CO_2[a]	L.O.I[b]
Magnesia	93.54	4.37	0.04	0.15	1.62	<0.02	<0.04	<0.007	<0.04	0.008	0.18	0.18
Wollastonite	0.41	51.86	0.86	0.19	44.15	0.12	0.31	0.019	0.05	0.009	0.50	1.99
KH_2PO_4	0.45	2.01	<0.3	0.007	<0.06	36.63	0.28	0.02	<0.024	40.44	n.d.[c]	20.94

[a] CO_2 content was calculated based on the total carbon content determined by combustion analyses.
[b] Loss on ignition.
[c] Not determined.

Table 2
Mix designs of the pastes used in this study referring to 100 g solid.

Sample	Mg/PO_4 molar ratio	w/b ratio	MgO [g]	KH_2PO_4 [g]	Wollastonite [g]	Water [g]	t_{FS}[a] [min]
P4-R	4	0.25	54.22	45.78	–	25	8 ± 1
P4-W	4	0.25	35.16	29.68	35.16	25	10 ± 1

[a] Final setting time as determined by the Vicat needle test using ~200 g paste.

600 °C at a heating rate of 10 °C/min using a Mettler Toledo TGA/SDTA 815e device under nitrogen atmosphere. Besides, TGA analyses on several wollastonite blended pastes (P4-W) samples after 108, 400 and 580 days were carried out from 30 to 1000 °C at a heating rate of 20 °C/min to determine possible additional hydrates from the reaction of the wollastonite. Based on the TGA results, the contents of K-struvite and $MgKPO_4{\cdot}H_2O$ of the hydrated MKP cements were quantified according to the method given in Appendix B, as well as the reaction degree of magnesia.

2.2.4. Nuclear magnetic resonance (NMR) spectroscopy

For solid-state nuclear magnetic resonance (NMR) spectroscopy, powder samples of hydrated pastes were prepared using the same protocol as given above for the XRD and TGA analyses. NMR spectra were acquired with a Bruker AV III HD 400 MHz wide-bore spectrometer. The ^{29}Si MAS NMR spectra were collected using a probe of 7 mm, at 79.505 MHz at a spinning speed of 4.5 KHz with a plus duration of 2.5 μs. The ^{31}P MAS NMR spectra were collected using a probe of 2.5 mm, at 161.995 MHz at a spinning speed of 20 KHz with a plus duration of 2.5 μs. Chemical shifts of ^{29}Si and ^{31}P were referenced to the external standards of tetramethylsilane ($Si(CH_3)_4$) and ammonium dihydrogen phosphate ($NH_4H_2PO_4$), respectively. The reaction degrees of wollastonite in the sample after 580 days at 20 °C and after 7 days at 20 °C and another 393 days at 50 °C are calculated based on the ^{29}Si NMR results as detailed in Appendix B.

2.2.5. Scanning electron microscopy

Backscattered electron (BSE) imaging coupled with energy dispersive X-ray spectroscopy (EDS) analyses were carried out on the wollastonite blended paste (P4-W) after 7 days curing at 20 °C plus 393 days at 50 °C. A small piece (diameter ~20 mm and height ~15 mm) was cut from the centre part of a paste cylinder, immersed in isopropanol for 1 week to remove all free water and stored at 40 °C for another 2 weeks to remove any remaining isopropanol. Afterwards, the paste was impregnated with a low viscosity epoxy resin, and a polished section was prepared by cutting and different steps of polishing. After a layer of 10 nm carbon coating, BSE imaging and EDS analyses were performed under high vacuum mode (3–4 × 10^{-6} Pa) with an accelerating voltage of 12 kV.

2.2.6. Thermodynamic modelling

Thermodynamic modelling was used to calculate the thermodynamically stable phases in pure and wollastonite blended MKP cement pastes in the temperature range of 5–100 °C at 1 bar. The geochemical software GEMS-PSI software [38,39] was used together with the PSI/Nagra thermodynamic database [40], the cement-specific database Cemdata18 database [41], completed with data for M-S-H and the recently complied database of magnesium (potassium) phosphate and calcium phosphates [11,42]; the Ca- and Mg-phosphate data used are summarised in Table 3.

The thermodynamic data between 5 and 100 °C at 1 bar were calculated using the temperature dependence of the apparent Gibbs free energy of formation as detailed below:

$$\begin{aligned}\Delta_a G_T^o &= \Delta_f G_{T_0}^o - S_{T_0}^o (T - T_0) - \int_{T_0}^{T}\int_{T_0}^{T} \frac{C_p^o}{T}\, dTdT \\ &= \Delta_f G_{T_0}^o - S_{T_0}^o (T - T_0) - a_0 \left(T\, ln\frac{T}{T_0} - T + T_0 \right) \\ &- 0.5a_1 (T - T_0)^2 - a_2 \frac{(T - T_0)^2}{2T \cdot T_0^2} - a_3 \frac{2\left(\sqrt{T} - \sqrt{T_0}\right)^2}{\sqrt{T_0}}\end{aligned} \quad (2)$$

where a_0, a_1, a_2, and a_3 are the empirical coefficients of the heat capacity equation $C_p^o = a_0 + a_1 T + a_2 T^{-2} + a_3\, T^{-0.5}$ and T_0 is the reference temperature (298.15 K). The apparent Gibbs free energy of formation $\Delta_a G_{T0}^o$ refers to the free energies of the elements at 298 K. The above calculation is built into the GEMS-PSI code. A more detailed description of the derivation of the dependence of temperature of the Gibbs free energy is given in the online documentation of GEMS by Kulik [46] or by Anderson and Crerar [47].

Table 3
Standard thermodynamic properties of magnesium, phosphate and potassium containing solids and structural water at 25 °C and 1 bar.

Species	log K°[a]	$\Delta_f G°$ [kJ/mol]	$\Delta_f H°$ [kJ/mol]	S° [J/mol/K]	$C_p°$ [J/mol/K]	Vol [cm^3/mol]	Ref[b]
Brucite $Mg(OH)_2$	16.84	−832.23	−923.27	63.14	77.28	24.6	[40]
Newberyite $MgHPO_4{\cdot}3H_2O$	−17.93	−2286.5	−2600.6	195.9	182.6	82.2	[23]
Phosphorrösslerite $MgHPO_4{\cdot}7H_2O$	−17.01	−3230.0	−3772.8	361.8	342.8	141.6	[23]
K-struvite $MgKPO_4{\cdot}6H_2O$	−10.96	−3240.8	−3717.3	350.1	324.8	142.5	[23]
$MgKPO_4{\cdot}H_2O$	−10.75[b]	−2053.6[b]	−2244.7[b]	141.3	124.6	66.1	[23]
$Mg_2KH(PO_4)_2{\cdot}15H_2O$	−28.67	−6949.1	−8086.7	781.6	747.6	303.2	[23]
Farringtonite $Mg_3(PO_4)_2$	−22.41	−3527.2	−3769.1	189.2	213.5	95.2	[23]
$Mg_3(PO_4)_2{\cdot}4H_2O$	−23.50	−4482.1	−4864.9	650.0	373.6	140.7	[23]
Bobierrite $Mg_3(PO_4)_2{\cdot}8H_2O$	−25.30	−5441.1	−6056.5	801.4	533.8	191.1	[23]
Cattiite $Mg_3(PO_4)_2{\cdot}22H_2O$	−23.03	−8748.7	−10,265.1	1046.6	1003.6	401.9	[23]
Hydroxyapatite $Ca_5(PO_4)_3(OH)$	−58.0	−6308.2	−6707.6	390.4[c]	385.2[c]	159.6	[11,43,44]
$CaK_3H(PO_4)_2$	−22.4	−3565.3	−3824.4	335[d]	276[d]	126.5	[11]

[a] Solubility products refer to reactions formulated with H^+, K^+, Mg^{2+}, Ca^{2+}, PO_4^{3-} and H_2O.
[b] The solubility of $MgKPO_4{\cdot}H_2O$ of −10.95 ± 1.5 could be defined more precisely to 10.75 ± 0.5 based on the observed transformation temperature reported in the paper.
[c] Entropy and heat capacity selected from [45].
[d] Entropy and heat capacity estimated from $CaHPO_4$, KH_2PO_4 and K_2HPO_4.

3. Results and discussion

3.1. Volume stability

The volume stabilities of the pastes without and with wollastonite under the different curing regimes are assessed in terms of linear length changes with time as shown in Fig. 1. The sample length changes at 20 °C and 70% R.H. within the first 7 days are detailed further in Fig. 1B. At 20 °C and 70% R.H. the reference paste (P4-R) shrinks during the first day of hydration; thereafter the lengths of the specimens increase with time, reaching an expansion of ~4.7‰ after 310 days. The observation is in line with a previous study [19] that showed MKP cement pastes with Mg/PO_4 molar ratio lower than 5 are likely to expand over time, due to the continuous hydration and hydrate transformation in the already hardened cement [6]. In contrast, the wollastonite-blended paste (P4-W) at 20 °C and 70% R.H. shrinks slightly with time reaching ~0.93‰ shrinkage after 461 days, indicating an improved volume stability in the presence of wollastonite. When the samples were stored at 50 °C after the 7 days of curing at 20 °C and 70% R.H., both pastes without and with wollastonite shrink similarly and significantly due to the increasing loss of free-water in the oven at 50 °C, where the relative humidity can drop below 20% [48,49], and due to the dehydration of K-struvite to be discussed in the following section.

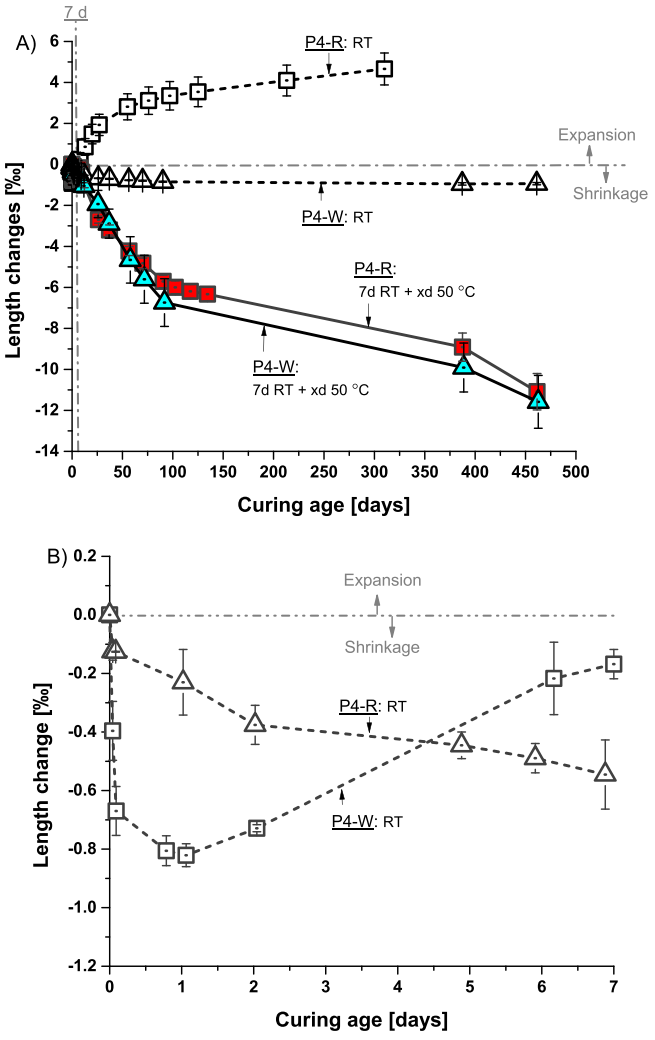

Fig. 1. Length changes of the pastes without (P4-R) and with wollastonite (P4-W) under the different curing regimes: A) during the entire curing period, B) within the first 7 days. Data of the reference paste at 20 °C and 70% R.H. (P4: RT) were taken from [6].

3.2. Mechanical strength

Fig. 2 shows the strength evolutions of the pastes without and with wollastonite under the different curing regimes used. As displayed in Fig. 2A, at 20 °C and 70% R.H. the reference paste (P4-R) shows a rapid compressive strength gain within the first 28 days but small strength changes thereafter. Compared to the reference paste (P4-R), the compressive strengths of the wollastonite-blended paste (P4-W) are lower at early ages, but much higher at late ages, in agreement with [11]. The curing at 50 °C after 7 days at 20 °C and 70% R.H. increases the compressive strengths of the pastes without and with wollastonite in a similar way up to a sample age of 28 days. However, longer curing times at 50 °C lead to a significant strength decrease of the reference paste (P4-R), while the compressive strengths of the wollastonite-blended cement (P4-W) continues to increase until 150 days and remains high thereafter.

Fig. 2B shows the flexural strength evolutions of the pastes, which are similar to the compressive strengths displayed in Fig. 2A. Compared with the reference paste (P4-R), the presence of wollastonite in MKP

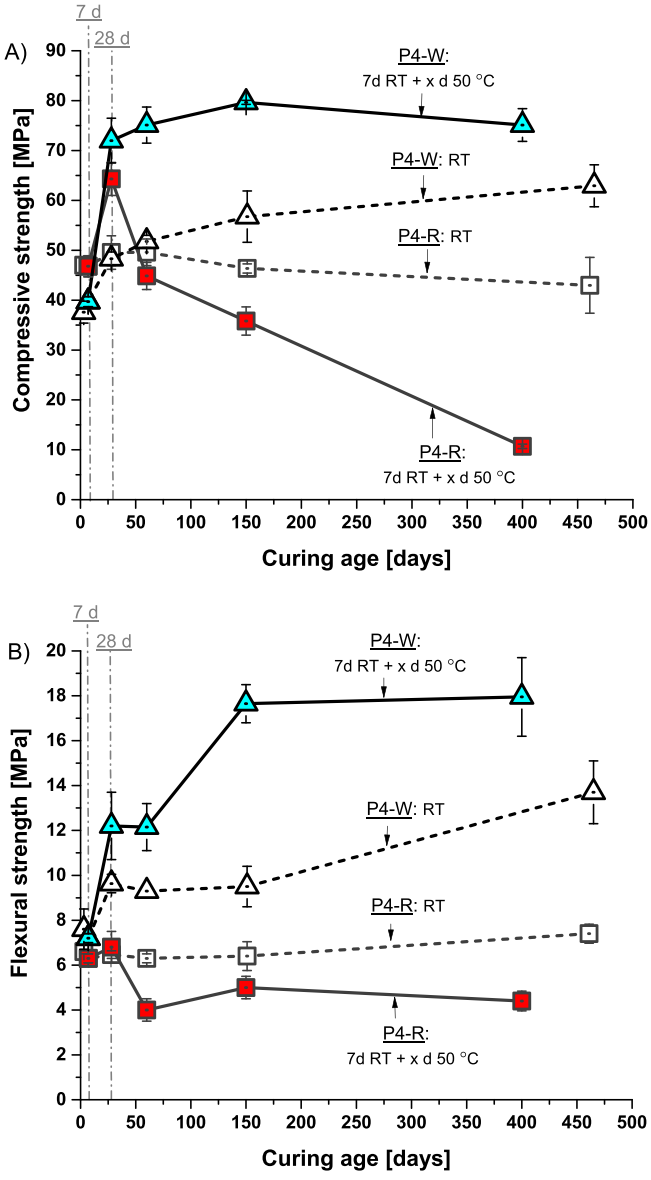

Fig. 2. Strength evolution of the pastes without (P4-R) and with wollastonite (P4-W) under the different curing regimes: A) compressive strength, B) flexural strength.

cement leads to much higher flexural strength with the increasing curing ages. In contrast to the strength decrease of the reference paste at higher temperature, the curing at 50 °C strongly increases the flexural strength of the wollastonite-blended cement (P4-W). The obtained mechanical results indicate that wollastonite plays an important role regarding strength contribution in general and prevention of strength decay at elevated temperature in particular.

3.3. Expected effect of temperature on hydrates

The reaction degrees of magnesia in the paste without (P4-R) and with wollastonite (P4-W) under the different curing regimes are estimated and summarised in Fig. 3. After 28 days roughly 20% of the magnesia present had reacted; the reaction degrees are increased slightly after 108 days, but no further increments are observed afterwards. It should be pointed out that the variations are within the 10% relative error range. The high relative error in particular for the 50 °C samples at later age are due to the partial decomposition of K-struvite in the samples. Based on the results in Fig. 3, the reaction degrees of magnesia used for the following thermodynamic calculations are 25% for the reference paste and 21% for the wollastonite-blended paste. The reaction degrees of wollastonite in the samples of the wollastonite-blended paste (P4-W) were estimated based on the ^{29}Si NMR results (see Appendix B) as 33 ± 5% for the sample after 580 days at 20 °C and as 30 ± 4% after 7 days at 20 °C plus 393 days at 50 °C. Thus, for the thermodynamic calculations it was assumed that the reaction degree of wollastonite slightly varies with temperature; an extension of the observed trend to 5 °C corresponds to ~34% and to 100 °C to a reaction degree of ~24%.

It is interesting to note that the reaction degree of wollastonite at 20 °C after 580 days at Mg/PO_4 molar ratio of 4 is lower than the reaction degree of wollastonite of 44 ± 6% at a Mg/PO_4 molar ratio of 2.7 (P2.7-W: 420d RT in Appendix B) [11]. This could be related to the much faster increase of pH during the hydration at higher Mg/PO_4 molar ratio [6,18] as wollastonite does not significantly react at pH values over 9 [28]. This lower reaction degree of wollastonite at high Mg/PO_4 molar ratio is also mirrored in a less strong strength increase in the presence of wollastonite observed here, compared to the stronger contribution to strength at Mg/PO_4 molar ratio of 2.7 [11].

The influence of the temperature in the range of 5–100 °C on the hydrate assemblages in the reference and wollastonite-blended pastes are calculated and illustrated in Fig. 4. Fig. 4A shows that mainly K-struvite, some $MgKPO_4{\cdot}H_2O$ (due to the limited availability of water), and traces of bobierrite and brucite are calculated as stable hydrates in

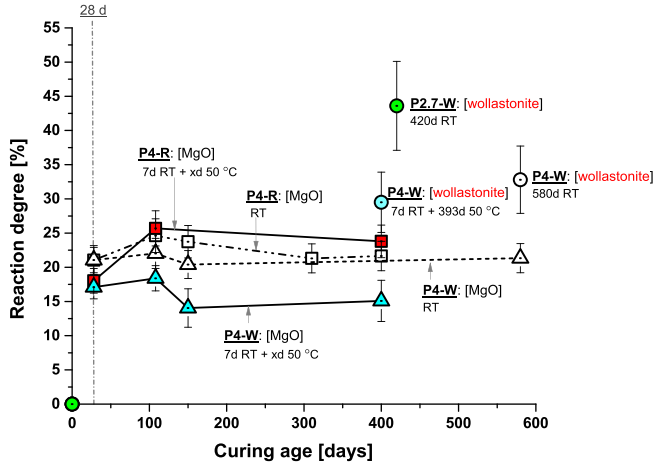

Fig. 3. Calculated reaction degrees of magnesia in the pastes (P4-R and P4-W) and of wollastonite in P4-W and P2.7-W [11] under the different curing regimes.

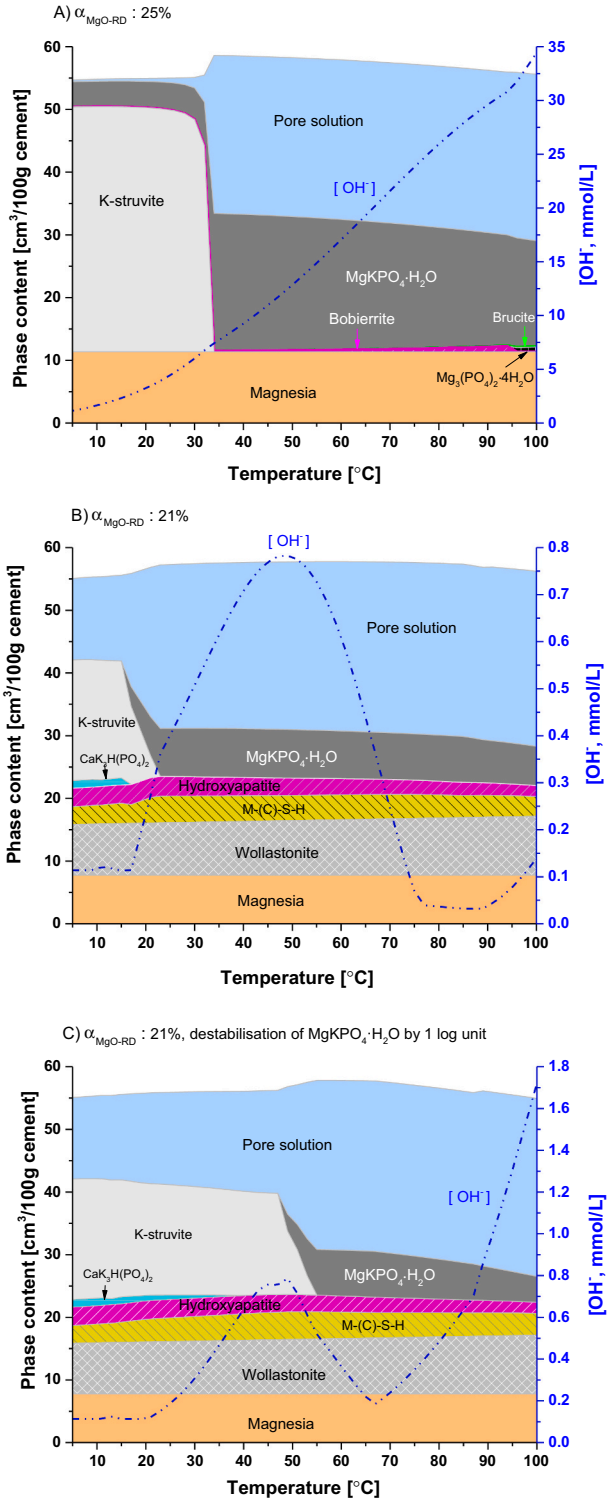

Fig. 4. Calculated thermodynamically stable solid phase assemblages in MKP cement pastes at w/b ratio of 0.25 in the temperature range of 5–100 °C. A) Reference paste without wollastonite. The expression 'cement' equals to magnesia + KH_2PO_4; B) and C) Wollastonite-blended paste. In C) the stability of $MgKPO_4$ H_2O was destabilised by 1 log unit to mimic kinetic hindrance. The expression 'binder' equals to magnesia + KH_2PO_4 + wollastonite.

the reference paste at 20 °C. At around 35 °C the destabilisation of K-struvite to $MgKPO_4{\cdot}H_2O$ is predicted, leading to a significantly lower volume of the solid phases. At higher temperatures slightly more bobierrite and brucite are calculated, and at temperatures above ~95 °C

bobierrite is transformed to $Mg_3(PO_4)_2{\cdot}4H_2O$.

In the presence of wollastonite, K-struvite is as well the main hydrate predicted at 20 °C as displayed in Fig. 4B, in addition to some M-(C)-S-H and hydroxyapatite, which in reality is rather amorphous hydroxyapatite as discussed in [11], and to small contents of $CaK_3H(PO_4)_2$ and C-S-H. The destabilisation of K-struvite is predicted at lower temperature than for the reference paste shown in Fig. 4A. The contents of M-(C)-S-H and hydroxyapatite are calculated to be slightly increased up to ~30 °C, and have small changes thereafter. However, if a destabilisation of $MgKPO_4{\cdot}H_2O$ by 1 log unit would be considered, $CaK_3H(PO_4)_2$ and K-struvite are calculated to remain stable up to ~42 °C and ~55 °C, respectively, as displayed in Fig. 4C. It can be speculated that the presence of Ca prevents kinetically the formation of $MgKPO_4{\cdot}H_2O$, similar to the Ca inhibition effect on K-struvite precipitation [50,51].

The comparison among Fig. 4A, B and C shows that the total solid phase volume of the wollastonite-blended paste is much less affected by a temperature increase from 20 to 50 °C due to the lower fraction of K-struvite and due to the presence of the thermally stable hydrates, hydroxyapatite and M-(C)-S-H, from the reaction of wollastonite [11]. The modelling results are in line with the observed high strength loss of the reference paste (P4-R) at 50 °C and with the high, well-maintained strengths of the wollastonite blended paste (P4-W) as displayed in Fig. 2.

3.4. Phase composition of the reference paste (P4-R)

As displayed in Fig. 5A, at 20 °C K-struvite is present in the hydrated paste (P4-R) at all the investigated ages together with traces of bobierrite after 400 days. Further traces of bobierrite and brucite are found in the sample at early ages (see Appendix C). The XRD findings of the reference paste at 20 °C are in good agreement with the thermodynamic calculations in Fig. 4A.

Fig. 5B shows that the curing at 50 °C leads to little changes of the hydrate assemblages after the short exposure time of 21 days, where K-struvite is still present; no $MgKPO_4{\cdot}H_2O$ is observed. However, possibly some K-struvite could be dehydrated to an amorphous phase as suggested in Appendix D. A prolonged curing at 50 °C leads to a partial dehydration of K-struvite to $MgKPO_4{\cdot}H_2O$ after 101 days and to an almost full dehydration after 393 days. The thermodynamic calculations in Fig. 4A suggest a significant decrease of the solid volume as $MgKPO_4{\cdot}H_2O$ forms instead of K-struvite. Thus, the observed progressive dehydration of K-struvite at 50 °C in the long-term explains the corresponding strength loss as demonstrated in Fig. 2. Again, the presence of bobierrite at 50 °C after 101 days agrees with the thermodynamic calculations in Fig. 4A, while the absence of bobierrite at other curing ages at 50 °C could be attributed due to a low content, which might be in the order of the detection limit of XRD analyses (approximately 1–5%).

The TGA results shown in Fig. 6A agree well with the XRD results in Fig. 5A, confirming the presence of mainly K-struvite at 20 °C. Traces of brucite are present after 310 and 400 days although no clear evidences are observed by XRD analysis. Generally, the bound water contents of the samples after 28, 108 and 150 days are similar; however, a slight decrease is observed for the samples after 310 and 400 days, indicating somewhat lower K-struvite contents due to unclear reasons.

For the samples exposed to 50 °C, K-struvite is dehydrated progressively to $MgKPO_4{\cdot}H_2O$ at 50 °C and less bound water content observed (Fig. 6B). In good agreement with the XRD initially K-struvite is present while $MgKPO_4{\cdot}H_2O$ is observed only after 101 days and longer. The formation of bobierrite is confirmed after 101 days at 50 °C, although the demonstrated characteristic DTG peak is shifted slightly to a lower temperature as compared to that of pure bobierrite at about 185 °C [23], due to the small content and/or the lower crystallinity [52]. Still a small and broad DTG hump of the sample after 393 days at 50 °C is observed in the range of approximately 50 to 150 °C, indicating the remaining traces of K-struvite.

Based on the TGA results, the volume fractions (in cm^3/100 g ignited

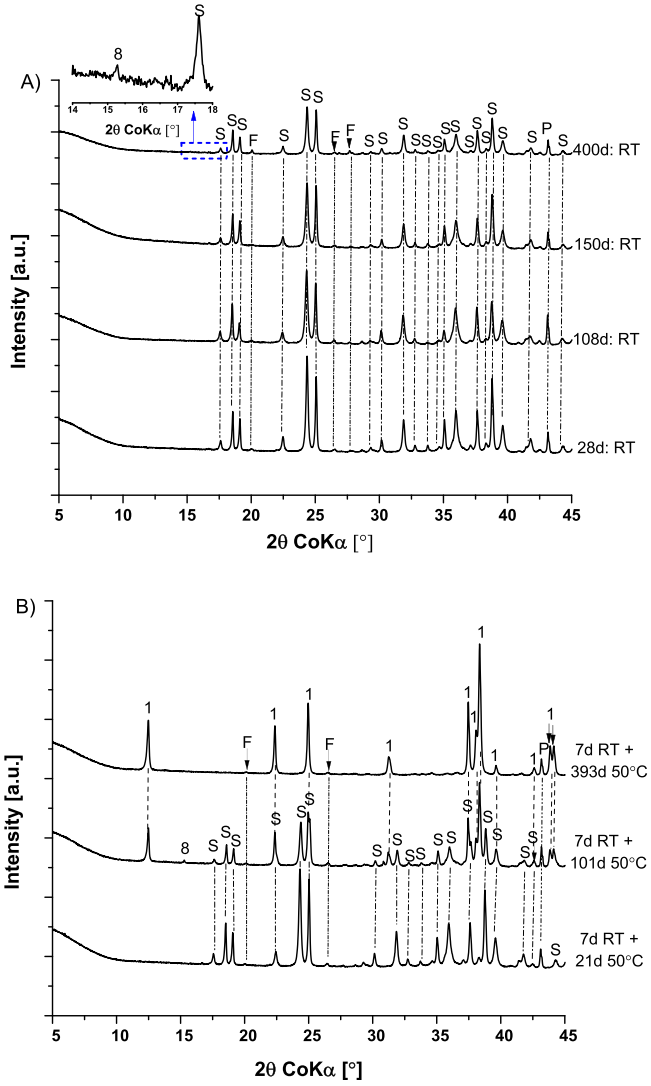

Fig. 5. XRD patterns of the reference paste (P4-R) under the different curing regimes of: A) curing at 20 °C, B) 7 days curing at 20 °C followed by a continuous curing at 50 °C for specific ages. 1 = $MgKPO_4{\cdot}H_2O$; 8 = bobierrite; F = forsterite; S = K-struvite; P = periclase.

paste) of K-struvite and $MgKPO_4{\cdot}H_2O$ in the paste under the different curing regimes are estimated and given in Fig. 7. While the volume of K-struvite decreases only slightly at 20 °C, the decrease of the hydrate volume at 50 °C is much more evident due to the significant dehydration of K-struvite to $MgKPO_4{\cdot}H_2O$. The obtained decrease of about 30% hydrate volume after 393 days at 50 °C agrees well with the thermodynamic calculations in Fig. 4A and the low strength in Fig. 2.

3.5. Phase composition of the wollastonite-blended paste (P4-W)

3.5.1. X-ray diffraction and thermogravimetric analysis

Also in the presence of wollastonite, K-struvite is the only crystalline hydrate in the paste at all the investigated ages, independent of the curing regimes as shown in Fig. 8. As detailed in [11], amorphous hydroxyapatite and M-(C)-S-H hydrates can form from the reaction of wollastonite in MKP cements (Mg/PO_4 molar ratio of 2.7, w/b ratios = 0.5 and 5), but are not clearly visible in the XRD patterns. In contrast to the (nearly) complete dehydration of K-struvite in the reference paste (P4-R) after 393 days at 50 °C (see Fig. 5B), K-struvite is preserved at 50 °C in the presence of wollastonite, although the intensities of the reflections decrease over time. The formation of $MgKPO_4{\cdot}H_2O$ is not

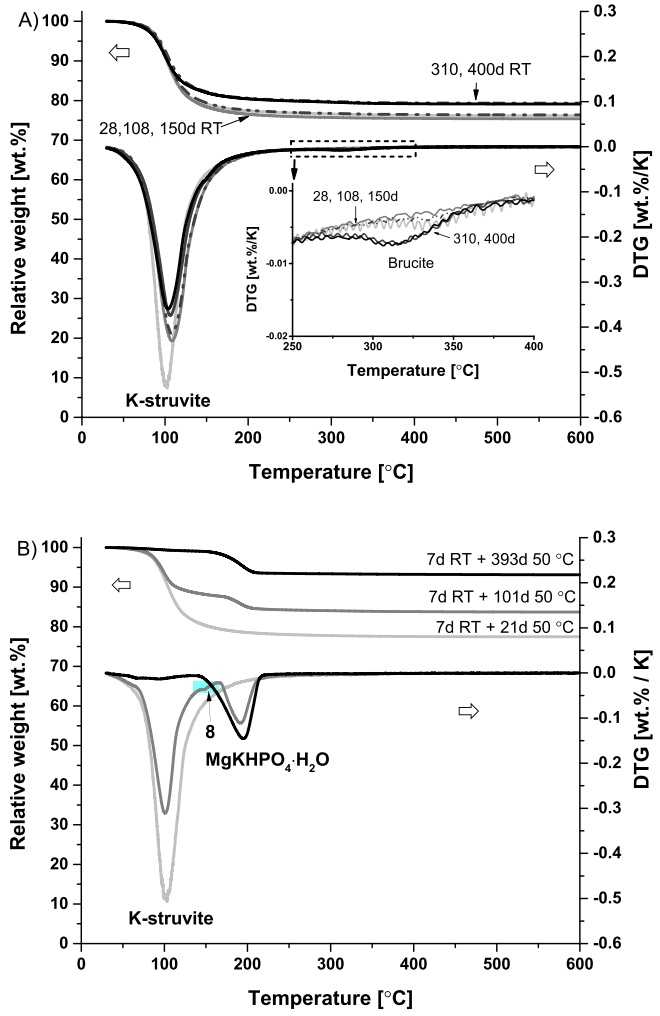

Fig. 6. TG/DTG curves of the hydrated reference paste (P4-R) under the different curing regimes of: A) curing at 20 °C, B) 7 days curing at 20 °C followed by a continuous curing at 50 °C for specific ages. 8 = bobierrite.

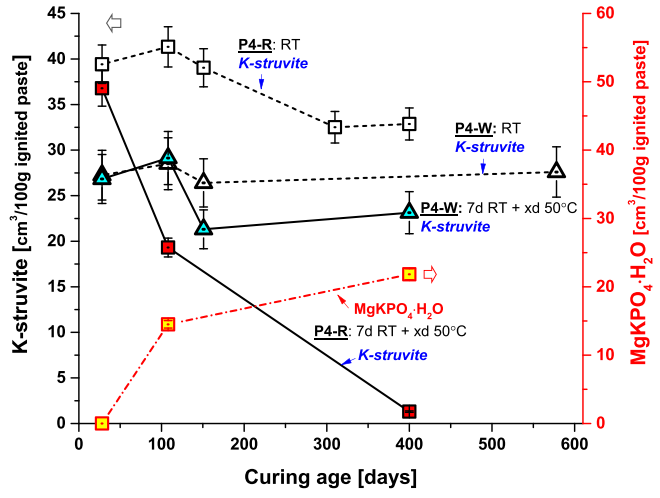

Fig. 7. Contents of K-struvite and $MgKPO_4 \cdot H_2O$ in the hydrated pastes without (P4-R) and with wollastonite (P4-W) in cm^3 per 100 g ignited paste under the different curing regimes used. The relative error considered is 10%.

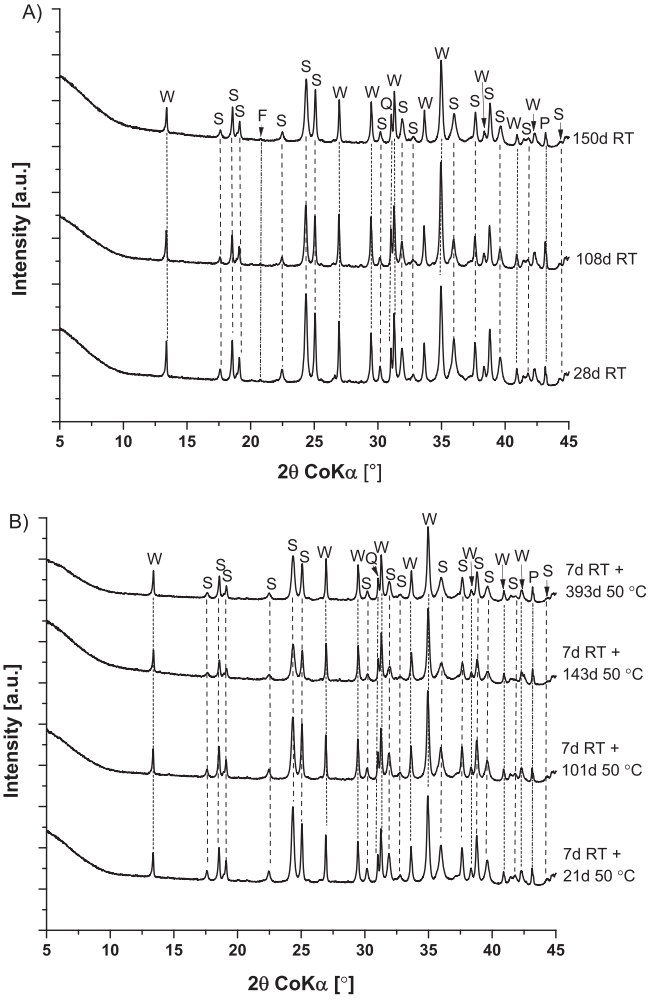

Fig. 8. XRD patterns of the wollastonite-blended paste (P4-W) under the different curing regimes of: A) curing at 20 °C, B) 7 days curing at 20 °C followed by a continuous curing at 50 °C for specific ages. F = forsterite; P = periclase; Q = quartz; S = K-struvite; W = wollastonite-2M.

observed, in contrast to the thermodynamic calculations shown in Fig. 4B. This indicates the significantly slower dehydration rate of K-struvite in the wollastonite-blended paste than in the reference paste, although some amorphous $MgKPO_4 \cdot H_2O$ might have formed, see Appendix D. The persistence of K-struvite in the paste agrees well with the long-term strength at 50°C as shown in Fig. 2.

The TGA results shown in Fig. 9 confirm the XRD findings. At 20 °C the bound water content (see Fig. 9A) is similar at all investigated ages, and the reaction degrees of magnesia as provided in Fig. 3 show small a little further reaction of magnesia after 28 days and later. It thus can be suggested that the observed continuous strength increase of the paste at later ages (see Fig. 2) could also be attributed to the formation of amorphous hydroxyapatite and M-(C)-S-H from the reaction of wollastonite [11]. Two minor DTG peaks at ~410 and ~650 °C are observed for the sample after 580 days at 20 °C, which could be assigned to traces of brucite and possibly to the formation of $CaK_3H(PO_4)_2$ [11]. At 50 °C the total bound water content decreases slightly with time (see Fig. 9B) indicating a minor dehydration of K-struvite, but no $MgKPO_4 \cdot H_2O$ in agreement with XRD. Also no additional DTG peaks are observed between 600 and 1000 °C.

The hydrate volume contents in the paste were estimated and provided in Fig. 7. In the presence of wollastonite the K-struvite contents are little affected by temperature. The K-struvite content remained stable at 20 °C, while only a small decrease of K-struvite content at 50 °C. This

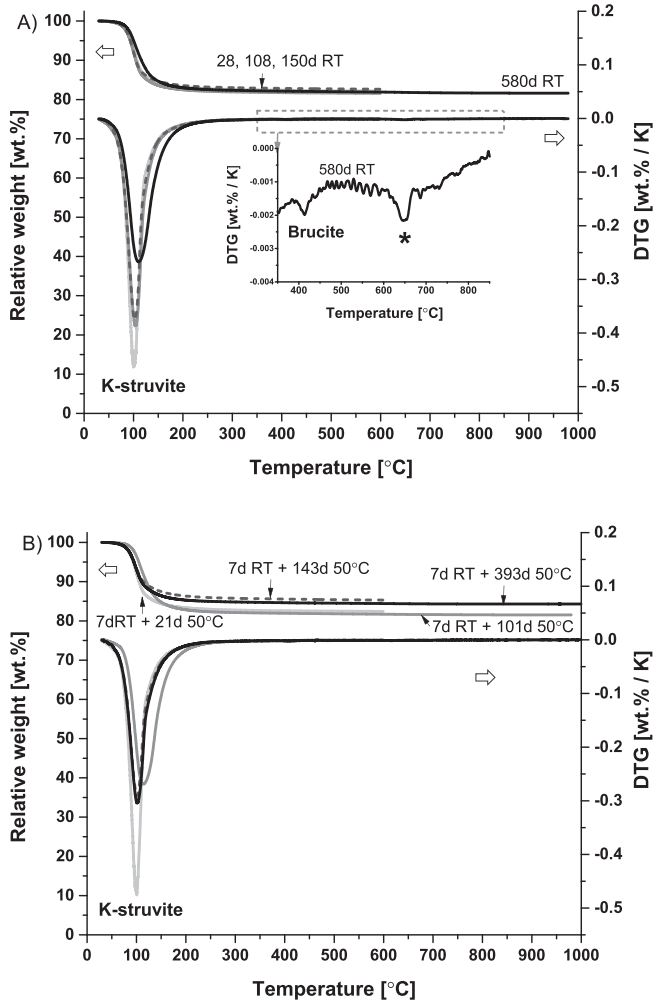

Fig. 9. TGA/DTG curves of the hydrated wollastonite-blended pastes (P4-W) under the different curing regimes of: A) curing at 20 °C, B) initial 7 days curing at 20 °C followed by a continuous curing at 50 °C for specific ages. * = unidentified phase.

decrease indicates that K-struvite in the wollastonite-blended paste is destabilized as suggested by the thermodynamic calculations (Fig. 4B), but much slower than in the reference paste.

3.5.2. NMR spectroscopy

The hydrates formed were further investigated by solid state NMR. The ^{31}P NMR spectrum of the wollastonite-blended paste (P4-W) after 393 days at 50 °C is shown in Fig. 10A. The sharp resonance peak at ~5.5 ppm corresponds to K-struvite [11] (see Appendix E). The broad hump at ~4 to 6 ppm indicates the presence of poorly ordered phosphates in agreement with [11]. The presence of (amorphous) hydroxyapatite and $CaK_3H(PO_4)_2$ could result in chemical shifts in this range (hydroxyapatite, δ: ~2.8 to 3.1 ppm [53,54]; $CaK_3H(PO_4)_2$, δ: 0 ppm [11]). However, it is difficult to clearly assess which phosphate might be present due to the overlap of the chemical shifts of various magnesium or calcium containing phosphates as summarised in Appendix E.

The ^{29}Si NMR spectra of an unhydrated wollastonite-blended cement (P2.7-W [11]: Mg/PO_4 molar ratio of 2.7, wollastonite content of 40%, by weight of binder) and two hydrated samples of P4-W under the different curing regimes in this study are shown in Fig. 10B. All the samples exhibit main resonances at ~−87.8 and −88.9 ppm corresponding to the Q^2 site of $CaSiO_3$ from wollastonite and minor resonances at about −61.6 (Q^0 site of Mg_2SiO_4), −65.8 ($CaMgSiO_4$ from magnesia) and −107.4 (Q^4 site of α-quartz, present as impurity in

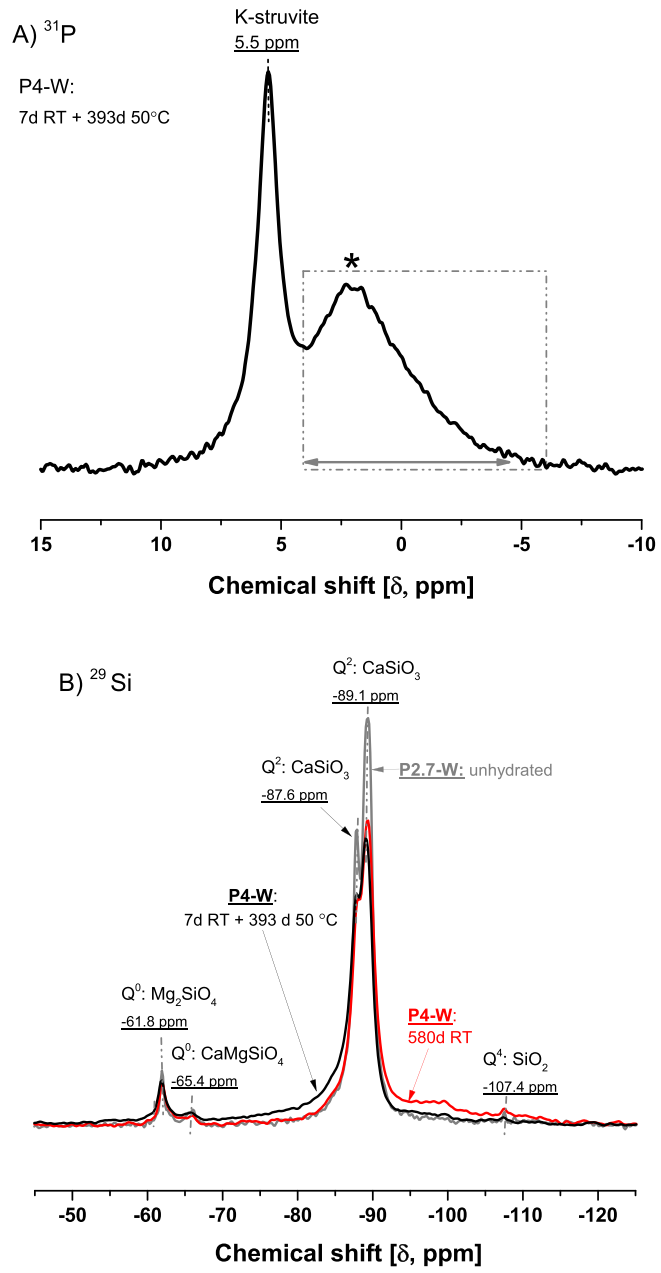

Fig. 10. NMR spectra of the wollastonite-blended cements: A) ^{31}P NMR spectrum of the sample (P4-W) after 7 days room temperature curing plus a continuous curing at 50 °C for 393 days, B) ^{29}Si spectra of an unhydrated wollastonite-blended MKP cement mixture (P2.7-W) [11] with a Mg/PO_4 molar ratio of 2.7 and a wollastonite content of 40%, by weight of binder, and of the hydrated sample (P4-W) after 580 days curing at 20 °C and of that 7 days curing at 20 °C followed by a continuous curing at 50 °C for 393 days.

wollastonite). As summarised in Appendix E, the chemical shifts of M-S-H and C-S-H solid solutions would overlap with those of wollastonite making a clear distinction difficult. However, the comparison with unreacted wollastonite [11], shows a broadening the bands between ~−75 and ~−100 ppm for the sample after 580 days at 20 °C and for the sample after 393 days at 50 °C. This points towards the reaction of wollastonite and towards the possible formation of M-(C)-S-H with several broad bands between ~−80 and ~−100 ppm [55,56], in agreement with the previous findings in [11] and with the thermodynamic calculations in Fig. 4B.

3.5.3. BSE/EDS analyses

The wollastonite blended paste (P4-W) after 7 days curing at 20 °C followed by a continuous curing at 50 °C for 393 days exhibits an intact and compact microstructure, consistent with its high strength shown in Fig. 2. The representative BSE image in Fig. 11A shows the presence of mainly K-struvite between unreacted magnesia and wollastonite particles. Additional phases are observed between the wollastonite particles (indicated by the arrows). Further different areas where K-struvite crystals are absent, are marked by numbers (1#, 2# and 3#) in Fig. 11A and B, which were further characterized by EDS.

Fig. 12A provides the measured K/P and Mg/P ratios obtained from EDS analyses. Some data points from the areas dominated by K-struvite (see Fig. 11A) show similar Mg/P and K/P ratios, indicating similar phase constituents; while the majority of data points in the areas dominated by K-struvite exhibit Mg/P ratios widely distributed between ~0.1 and ~1.1, mainly clustered into two zones. An Mg/P ratio of 0.5 was arbitrarily selected as the boundary value in order to calculate the average Mg/P and K/P ratios of each zone of data points. The calculated average Mg/P and K/P ratios as given in Fig. 12A are 0.3 ± 0.1 and 0.7 ± 0.1 for zone I, and 0.8 ± 0.2 and 0.8 ± 0.1 for zone II, which are close to the stoichiometric values of K-struvite and $MgKPO_4·H_2O$.

In the areas dominated by K-struvite (see Fig. 11A), the Ca/(Ca + Mg) ratios are between ≈0.1 and 1 and the P/(Ca + Mg) ratios mostly below 1, indicating a mix of wollastonite, magnesium phosphate hydrates and calcium phosphate hydrates. Hydroxyapatite rather than octacalcium phosphate is likely to form based on the thermodynamic calculations in Fig. 4B and previous findings [11]. The magnesium phosphate hydrates without calcium shown in Fig. 12B have a measured P/Mg ratios > 1, in good agreement with the previous EDS results on K-struvite hydrates present in pure MKP cement matrices [6,18].

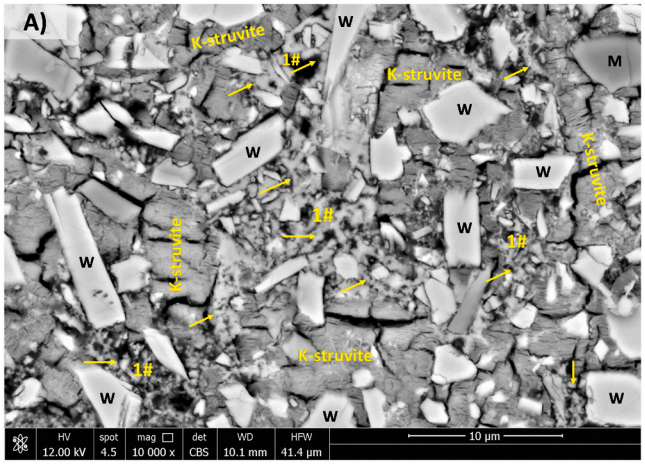

Fig. 11. Typical BSE images of the wollastonite-blended paste (P4-W) after 7 days curing at 20 °C followed by a continuous curing at 50 °C for 393 days. M = magnesia, W = wollastonite.

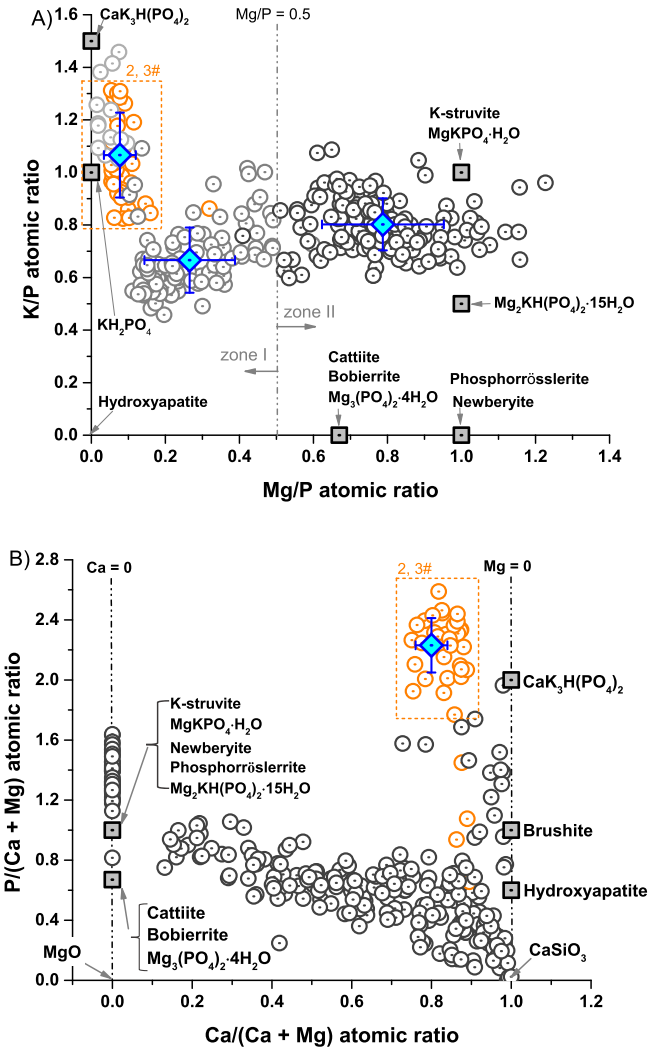

Fig. 12. EDS analyses of solids in the wollastonite blended paste (P4-W) after 7 days curing at 20 °C followed by a continuous cuing at 50 °C for 393 days. The grey datasets are from the areas dominated by K-struvite (see Fig. 11A), and the orange datasets are from the areas dominated by the dissolution of wollastonite (see 2# and 3# in Fig. 11B).

The areas 2# and 3# in Fig. 11A show a lower average Mg/P ratio of ~0.08 ± 0.04 and a relatively high average K/P ratio of ~1.1 ± 0.2, pointing towards a possible mix of $CaK_3H(PO_4)_2$ and magnesium phosphate hydrates in the areas where originally reacted wollastonite had been present. In the areas 2# and 3# in Fig. 11B the average Ca/(Ca + Mg) and P/(Ca + Mg) ratios are 0.8 ± 0.04 and 2.2 ± 0.2, as shown in Fig. 12B.

3.5.4. Effect of Mg/PO_4 on the hydrates formed

In a previous study [11] with a lower Mg/PO_4 (Mg/PO_4 molar ratio of 2.7, w/b = 0.5 and 5) only hydroxyapatite was observed to form in the presence of wollastonite, whereas here also $CaK_3H(PO_4)_2$ is present after 393 days at 50 °C. Hydroxyapatite and $CaK_3H(PO_4)_2$ can co-precipitate together in wollastonite-KH_2PO_4 suspensions at early age as shown in Appendix F, but $CaK_3H(PO_4)_2$ is expected to be destabilized in the long-term to hydroxyapatite through reaction (12) if sufficient [OH^-] is available as discussed in [11]:

$$5CaK_3H(PO_4)_2 + 6OH^- \rightarrow Ca_5(PO_4)_3OH + 15\ K^+ + 7PO_4^{3-} + 5H_2O \quad (3)$$

In the presence of wollastonite, hydroxyapatite could also originate from the destabilisation of K-struvite [11]. When a M-S-H composition of $Mg_{0.75}SiO_{2.75}(H_2O)_{1.25}$ is considered, the reaction can be written as follows.

$$3MgKPO_4{\cdot}6H_2O + 5CaSiO_3 \rightarrow Ca_5(PO_4)_3OH + 4\ M-S-H + SiO_2\ (amorphous) + 3\ K^+ + 3OH^- + 11H_2O \quad (4)$$

This reaction could also be a reason for the decrease of the amount of K-struvite in the wollastonite-blended paste at 50 °C (see Figs. 8B and 9B), in addition to the possible formation of amorphous magnesium phosphate hydrates (Appendix D), in particular as we observe a higher reaction of wollastonite at higher temperature.

Compared with K-struvite, hydroxyapatite, M-S-H and $CaK_3H(PO_4)_2$ degrade less easily with temperature; their presence in the MKP cement matrix contributes together with the high wollastonite reaction to the intact microstructure (see Fig. 11) at 50 °C and the long-term high strengths (see Fig. 2).

4. Conclusions

In this study, the influence of curing at 20 and 50 °C on the properties and the hydrations of MKP cement pastes without and with wollastonite was investigated through a series of experimental characterizations and thermodynamic modelling. The main findings of this work can be summarised as in the following:

- Impact on strength and volume stability

The samples of MKP only and those of blends with wollastonite showed both a good strength development at 20 °C, both of the early strength as well as in the long-term. In the presence of wollastonite, the strength was somewhat higher than in the absence of wollastonite and continued to increase up to more than 1 year. At 20 °C, wollastonite was observed to stabilize the volume of hydrated cements in the long-term, and only a small shrinkage was observed.

- Impact on the hydrate assemblages

At 20 °C K-struvite (and traces of bobierrite and brucite) form in the paste. In contrast at 50 °C K-struvite is destabilized progressively to $MgKPO_4{\cdot}H_2O$ with increasing curing age. The destabilisation of K-struvite to $MgKPO_4{\cdot}H_2O$ leads to a significantly lower volume of the solid phase and thus to a significantly lower strength.

In the wollastonite-blended paste, K-struvite is the main hydrate. The destabilisation of K-struvite to $MgKPO_4{\cdot}H_2O$ at 50 °C seems to be kinetically hindered, possibly due to the presence of Ca from wollastonite reaction and occurs at a significantly slower rate than in MKP paste. The reaction of wollastonite leads to the precipitation of amorphous Ca-phosphates (possibly amorphous hydroxyapatite), $CaK_3H(PO_4)_2$, and M-(C)-S-H. The presence of K-struvite together with amorphous hydroxyapatite, $CaK_3H(PO_4)_2$ and M-(C)-S-H at 50 °C is responsible for the stable high strengths of the wollastonite-blended MKP cement under the long-term curing.

The phase developments predicted by thermodynamic modelling in pure and wollastonite-blended MKP cements in the temperature range of 5–100 °C agree generally well with the experimental findings, with exception of the very slow destabilisation of K-struvite in the presence of wollastonite at 50 °C, which seems to indicate some kinetic hindrance of the reaction and should be further investigated.

CRediT authorship contribution statement

Biwan Xu: Investigation, Writing - original draft. **Frank Winnefeld:** Writing - review & editing. **Barbara Lothenbach:** Funding acquisition, Project administration, Writing - review & editing.

Declaration of competing interest

The authors declare that they have no known competing financial interests or personal relationships that could have appeared to influence the work reported in this paper.

Acknowledgements

The financial support of Saint-Gobain Recherche, France, is gratefully acknowledged as well as the constructive suggestions of Céline Cau Dit Coumes (CEA, France), Andreas Leemann (Empa, Switzerland), Raül Leiva Muñoz and Nelly Brielles (Saint-Gobain Recherche, France). Our thank is extended to Boris Ingold (Empa) for the SEM sample preparation, to Daniel Rentsch (Empa) for acquiring the ^{29}Si and ^{31}P MAS NMR spectra and to Robin Pauer (Empa) for the assistance with the SEM characterizations. The NMR hardware was partially granted by the Swiss National Science Foundation (SNSF, grant no. 206021_150638/1).

Appendix A

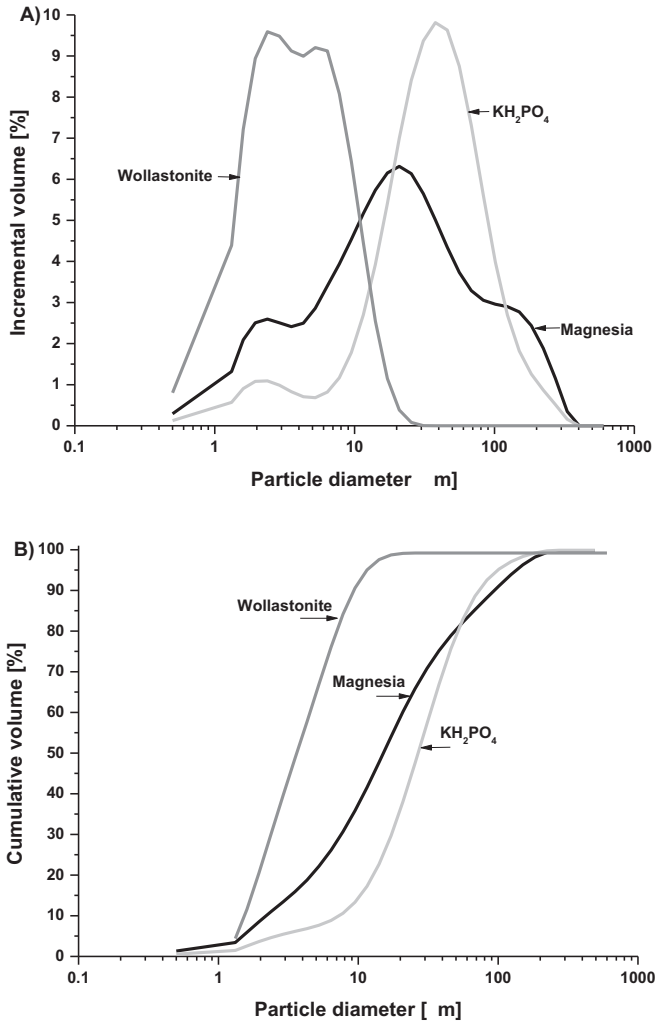

Fig. A. Particle size distribution of the staring materials. A) Differential particle size distribution, B) cumulative particle size distribution.

Appendix B

- Calculations of contents of K-struvite and $MgKPO_4{\cdot}H_2O$ and magnesia reaction degree

The contents of K-struvite and $MgKPO_4{\cdot}H_2O$ were quantified based on their weight loss and calculated according to the following equations:

$$K\_struvite_{dry} = \frac{W_{water-kstr}}{W_{600^\circ C}} \times \frac{M_{Kstr}}{6 \times M_{H_2O}} \times \frac{100}{\rho_{Kstr}} = \frac{W_{water-kstr}}{W_{600^\circ C}} \times \frac{266.5}{108} \times \frac{100}{1.87} \quad \text{(A1)}$$

$$MKP{\cdot}H_{dry} = \frac{W_{water-MKP{\cdot}H}}{W_{600^\circ C}} \times \frac{M_{MKP{\cdot}H}}{M_{H_2O}} \times \frac{100}{\rho_{MKP.H}} = \frac{W_{water-MKP{\cdot}H}}{W_{600^\circ C}} \times \frac{176.4}{18} \times \frac{100}{2.67} \quad \text{(A2)}$$

where $K\_struvite_{dry}$ and $MKP \cdot H_{dry}$ represent the volume of K-struvite and $MgKPO_4{\cdot}H_2O$ in cm^3/100 g ignited paste; $W_{water-Kstr}$ is the weight loss of K-struvite from 30 to 210 °C (except for the reference pure paste (P4-R) after 101 and 393 days cured at 50 °C, where the weight losses from 30 to 165 °C and from 30 to 140 °C were used due to the presence of $MgKPO_4{\cdot}H_2O$); $W_{water-MKP{\cdot}H}$ is the weight loss of $MgKPO_4{\cdot}H_2O$ for the reference paste (P4-R) from 165 to 220 °C for the samples after 101 days at 50 °C and from 140 to 220 °C for that after 393 days at 50 °C; $W_{600^\circ C}$ is the ignited weight of the hydrated paste at 600 °C; M_{Kstr}, $M_{MKP{\cdot}H}$ and M_{H2O} are the molar masses of K-struvite, $MgKPO_4{\cdot}H_2O$ and water, equal to 266.5, 176.4 and 18 g/mol, respectively; ρ_{Kstr} and $\rho_{MKP.H}$ are the densities of K-struvite and $MgKPO_4{\cdot}H_2O$, equal to 1.87 and 2.67 g/cm^3, respectively [23]. It should be noted that the temperature ranges of the hydrates could slightly vary depending on several factors such as different heating rates, sample amounts used and hydrate contents in sample [52].

Following the method detailed in [8,57], magnesia reaction degree of the hydrated reference (P4-R) and wollastonite blended pastes (P4-W) can be estimated based on the weight loss of the formed hydrates, which includes the amount of K-struvite, $MgKPO_4{\cdot}H_2O$, bobierrite ($Mg_3(PO_4)_2{\cdot}8H_2O$) and brucite ($Mg(OH)_2$) based on the XRD and TGA results presented in the following section. The corresponding reacted magnesia contents are calculated through the following equations:

$$W_{MgO-Kstr} = \frac{W_{water-Kstr}}{W_{600^\circ C}} \times \frac{M_{MgO}}{6 \times M_{H_2O}} \times 100 = \frac{W_{water-Kstr}}{W_{600^\circ C}} \times \frac{40.3}{6 \times 18} \times 100 \quad (A3)$$

$$W_{MgO-MKP\cdot H} = \frac{W_{water-MKP\cdot H}}{W_{600^\circ C}} \times \frac{M_{MgO}}{M_{H_2O}} \times 100 = \frac{W_{water-MKP\cdot H}}{W_{600^\circ C}} \times \frac{40.3}{18} \times 100 \quad (A4)$$

$$W_{MgO-Bob} = \frac{W_{water-Bob}}{W_{600^\circ C}} \times \frac{3 \times M_{MgO}}{8 \times M_{H_2O}} \times 100 = \frac{W_{water-Bob}}{W_{600^\circ C}} \times \frac{3 \times 40.3}{8 \times 18} \times 100 \quad (A5)$$

$$W_{MgO-MH} = \frac{W_{water-MH}}{W_{600^\circ C}} \times \frac{M_{MgO}}{M_{H_2O}} \times 100 = \frac{W_{water-MH}}{W_{600^\circ C}} \times \frac{40.3}{18} \times 100 \quad (A6)$$

where $W_{water-Bob}$ is the weight loss of bobierrite from 140 to 165 °C for the reference paste (P4-R) after 101 days at 50 °C; $W_{water-MH}$ is the weight loss of brucite from 250 to 450 °C for the pastes at 20 °C; M_{MgO} is the molar mass of magnesia, equal to 40.3 g/mol.

Thus, the total reacted magnesia ($W_{MgO-reacted}$) can be summed through the following equation:

$$W_{MgO-reacted} = W_{MgO-Kstr} + W_{MgO-MKP\cdot H} + W_{MgO-Bob} + W_{MgO-MH} \quad (A7)$$

The weight of the ignited paste was assumed equal to the sum of magnesia and KPO_3 and wollastonite. Thus, based on the Eqs. (A1)–(A7) the reaction degree of magnesia in the hydrated reference and wollastonite blended pastes can be calculated and written through the following general equation:

$$\partial_{\mathrm{MgO-RD}} = \frac{W_{MgO-reacted}}{W_{MgO-total}} \times 100\% \quad (A8)$$

- Calculation of wollastonite reaction degree

Reaction degree of Si-containing phases in Portland cement blends such as alite, belite and metakaolin can be determined by deconvoluting ^{29}Si NMR spectra [58]. Deconvolutions were carried out on the measured ^{29}Si NMR spectra of unhydrated / hydrated wollastonite-blended MKP cements. The deconvolution of the unhydrated wollastonite-blended cement (P2.7-W: unhydrate) is displayed in Fig. B.

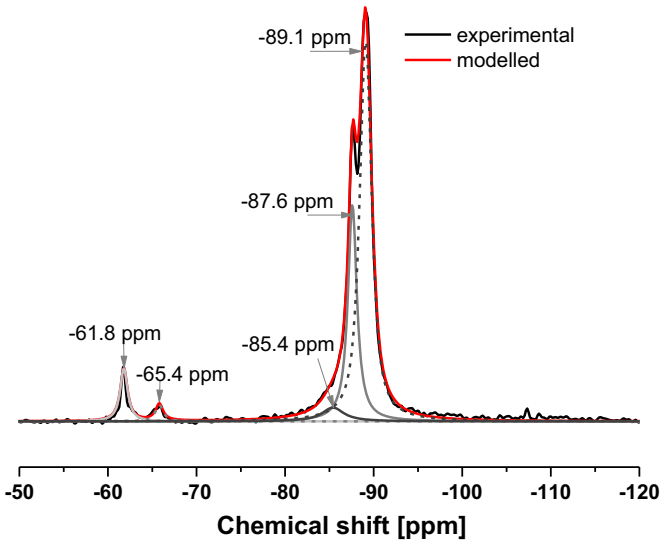

Fig. B. Deconvolution of the ^{29}Si NMR spectra of the sample P2.7-W: unhydrated. The deconvoluted curves at −85.4, −87.6 and −89.1 ppm were for the Si present in wollastonite, while these at −61.8 and −65.4 ppm were for the impurities (i.e. Mg_2SiO_4 and $CaMgSiO_4$) in magnesia.

The populations [Pop.] due to the presence of Si in wollastonite are summarised in Table B, as well as the reaction degrees of wollastonite [α_{CaSiO3}] in the samples, which are calculated through.

$$\alpha_{CaSiO3} = \left(1 - P_{total-hydrated} / P_{total-unhydrated}\right) \times 100\% \quad (A9)$$

where $P_{total-unhydrated}$ is the sum of the populations [Pop.] at −85.4, −87.6 and −89.1 ppm of the unhydrated wollastonite-blended cement (P2.7-W: unhydrated); and $P_{total-hydrated}$ is the sum for the hydrated samples. In all cases, the position and the width of the signals related to wollastonite was kept constant.

Table B
Calculated reaction degree of wollastonite [α_{CaSiO3}] based on the deconvolution results.

Wollastonite		Pop. [%]				
δ [ppm]	FWHM[a]	G/L[a]	P2.7-W: Unhydrated	P2.7-W: 420d RT[b]	P4-W: 580d RT	P4-W: 7d RT + 393d 50 °C
−85.4	3.00	0	4.3	7.8[c]	2.3	7.8[c]
−87.6	1.20	0	27.5	13.8	19.1	18.6
−89.1	1.62	0.2	60.9	30.6	40.8	38.9
P_{total} [%]		*92.6*		*52.2*	*62.2*	*65.3*
α_{CaSiO3} [%]		0		43.6[d]	32.8	29.5[d]

Note: [a]: FWHM: Full Width at Half Maximum; G/L: ratio of Gaussian to Lorentzian. [b]: the ^{29}Si NMR spectra was shown in [11]. [c]: compared to the unhydrated sample, the increased Pop. values at −85.4 ppm indicate the possible formation of Si-containing hydrates; therefore, [d]: the calculated reaction degrees of the samples P2.7-W: 420d RT and P4-W: 7d RT + 393d 50 °C are somewhat underestimated. Relative error of ±15% is considered. The values in italic represent the sum of the fraction of wollastonite observed by NMR.

Appendix C

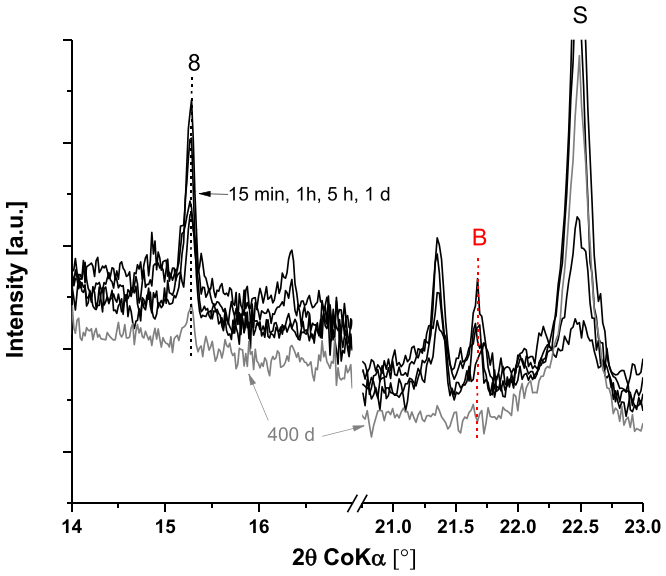

Fig. C. XRD patterns of the reference cement paste (P4-R). 8 = bobierrite, B = brucite, S = K-struvite.

Appendix D

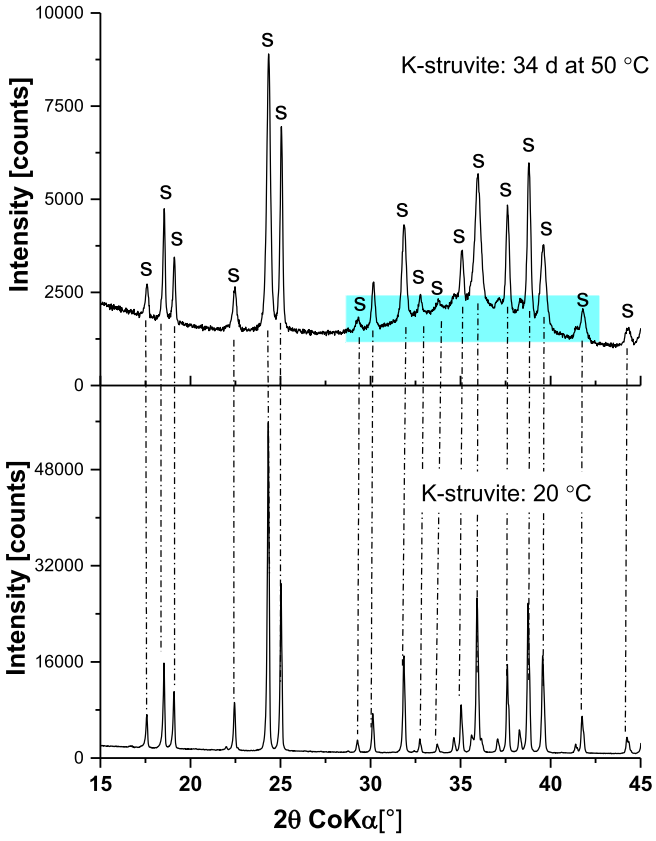

Fig. D. XRD patterns of K-struvite before and after drying in open vessel at 50 °C for 34 days. As compared to K-struvite at 20 °C, the intensities of the K-struvite reflections after 34 days at 50 °C are strongly decreased, while no $MgKPO_4{\cdot}H_2O$, but an amorphous phase as indicated by the broad hump (marked in light blue) was observed. The preparation of K-struvite is detailed in [18].

Appendix E

Table E
Summary of ^{31}P MAS NMR data for magnesium, calcium, and potassium containing phosphates and ^{29}Si MAS NMR data for silicate containing phases taken from literature.

Mineral	^{31}P	Mineral	^{29}Si
	δ [ppm]		δ [ppm]
KH_2PO_4	3.6 [59], 3.9 [10]	Wollastonite: *β-$Ca_3Si_3O_9$*	−89.0 ± 0.2, −89.5 ± 0.2, −87.8 ± 0.2 [60,61]
Newberyite: *$MgHPO_4{\cdot}3H_2O$*	−7.5 [10], −8 [62]	Forsterite: *Mg_2SiO_4*	−62 [11,63]
Phosphorrösslerite: *$MgHPO_4{\cdot}7H_2O$*	1.7 [10]	Monticellite: *$CaMgSiO_4$*	−66 [11]
K-struvite: *$MgKPO_4{\cdot}6H_2O$*	5.6 [11], 6.2 [59], 6.4 [10]	Quartz: *α-SiO_2*	−107.4 [52,64]
		M-S-H: *Mg/Si = 0.8–1.2*	≈−79–−97 [55,56], e.g. −78.3, −85.5, −92.7, −93.5 −94.7, −96.7 ± 0.3 [56]
$Mg_2KH(PO_4)_2{\cdot}15H_2O$	2.8 [10]	C-S-H: *Ca/Si = 0.7–1.5*	≈−79–−88 [55,65,66], e.g. −79.4, −82.9, −85.5, −88.4 [55]
Bobierrite: *$Mg_3(PO_4)_2{\cdot}8H_2O$*	4.6 [10,67]		
Cattiite[a]: *$Mg_3(PO_4)_2{\cdot}22H_2O$*	1.1 [67], 6.9 [10]		
Farringtonite: *$Mg_3(PO_4)_2$*	−0.5 [67]		
Brushite: *$CaHPO_4{\cdot}2H_2O$*	1.6 [54], 1.7 [68]		
Octacalcium phosphate: *$Ca_8H_2(PO_4)_6{\cdot}5H_2O$*	−0.2, 2.0, 3.3, 3.7 [69]		
Hydroxyapatite: *$Ca_5(PO_4)_3(OH)$*	2.81 ± 0.10, 2.90 ± 0.10 [53], 3.1 [68]		
$CaK_3H(PO_4)_2$	0 [11]		

[a] The chemical shifts of cattiite documented in [10,67] differ strongly, and thus more experimental data are needed for further confirmation.

Appendix F

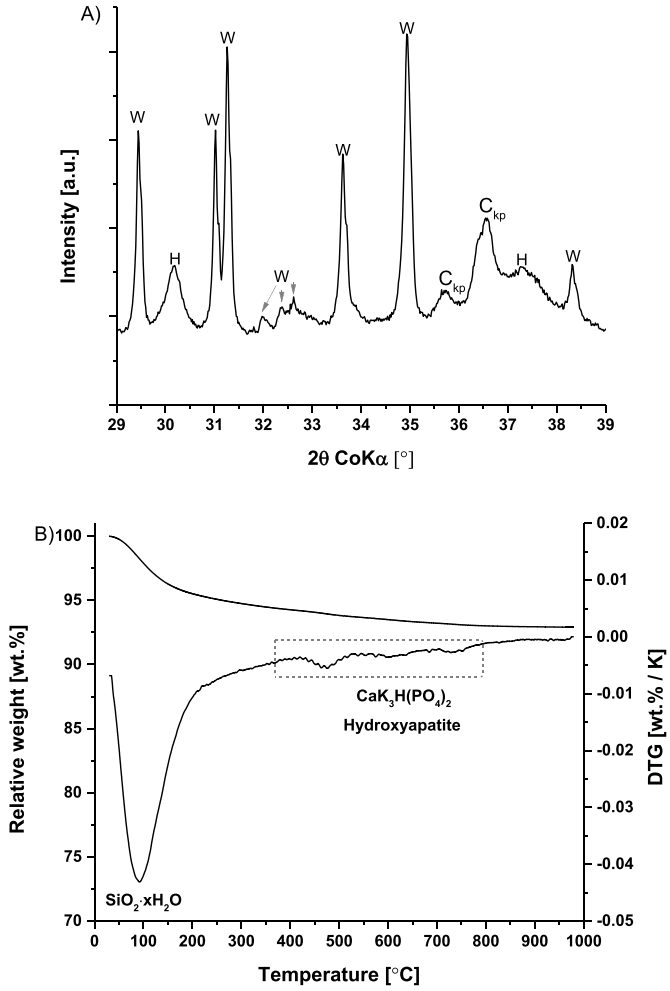

Fig. F. Analyses of the reaction products of wollastonite in KH_2PO_4 solution after 28 days at 20 °C. A) XRD pattern: W = wollastonite-2M, H = hydroxyapatite, C_{kp} = $CaK_3H(PO_4)_2$; B) TGA/DTG curves. Note: mass ratio of wollastonite: KH_2PO_4: water = 1.2: 1: 15.

References

[1] A.S. Wagh, Chapter 9 - magnesium phosphate ceramics, in: A.S. Wagh (Ed.), Chemically Bonded Phosphate Ceramics, Elsevier, Oxford, 2004, pp. 97–111.
[2] S.A. Walling, J.L. Provis, Magnesia-based cements: a journey of 150 years, and cements for the future? Chem. Rev. 116 (2016) 4170–4204.
[3] F. Qiao, C.K. Chau, Z. Li, Property evaluation of magnesium phosphate cement mortar as patch repair material, Constr. Build. Mater. 24 (2010) 695–700.
[4] B. Xu, H. Ma, H. Shao, Z. Li, B. Lothenbach, Influence of fly ash on compressive strength and micro-characteristics of magnesium potassium phosphate cement mortars, Cem. Concr. Res. 99 (2017) 86–94.
[5] B. Xu, B. Lothenbach, H. Ma, Properties of fly ash blended magnesium potassium phosphate mortars: effect of the ratio between fly ash and magnesia, Cem. Concr. Compos. 90 (2018) 169–177.
[6] B. Xu, F. Winnefeld, J. Kaufmann, B. Lothenbach, Influence of magnesium-to-phosphate ratio and water-to-cement ratio on hydration and properties of magnesium potassium phosphate cements, Cem. Concr. Res. 123 (2019) 105781.
[7] Y. Li, W. Bai, T. Shi, A study of the bonding performance of magnesium phosphate cement on mortar and concrete, Constr. Build. Mater. 142 (2017) 459–468.
[8] B. Xu, H. Ma, Z. Li, Influence of magnesia-to-phosphate molar ratio on microstructures, mechanical properties and thermal conductivity of magnesium potassium phosphate cement paste with large water-to-solid ratio, Cem. Concr. Res. 68 (2015) 1–9.
[9] H. Lahalle, C. Cau Dit Coumes, A. Mesbah, D. Lambertin, C. Cannes, S. Delpech, S. Gauffinet, Investigation of magnesium phosphate cement hydration in diluted suspension and its retardation by boric acid, Cem. Concr. Res. 87 (2016) 77–86.
[10] H. Lahalle, C. Cau Dit Coumes, C. Mercier, D. Lambertin, C. Cannes, S. Delpech, S. Gauffinet, Influence of the w/c ratio on the hydration process of a magnesium phosphate cement and on its retardation by boric acid, Cem. Concr. Res. 109 (2018) 159–174.
[11] B. Xu, B. Lothenbach, F. Winnefeld, Influence of wollastonite on hydration and properties of magnesium potassium phosphate cements, Cem. Concr. Res. 131 (2020) 106012.
[12] I. Buj, J. Torras, D. Casellas, M. Rovira, J. de Pablo, Effect of heavy metals and water content on the strength of magnesium phosphate cements, J. Hazard. Mater. 170 (2009) 345–350.
[13] I. Buj, J. Torras, M. Rovira, J. de Pablo, Leaching behaviour of magnesium phosphate cements containing high quantities of heavy metals, J. Hazard. Mater. 175 (2010) 789–794.
[14] Y. He, Z. Lai, T. Yan, X. He, Z. Lu, S. Lv, F. Li, X. Fan, H. Zhang, Effect of Cd^{2+} on early hydration process of magnesium phosphate cement and its leaching toxicity properties, Constr. Build. Mater. 209 (2019) 32–40.
[15] Z. Zhang, Z. Yang, Z. Chen, T. Kang, X. Ding, Y. Li, Y. Liao, C. Chen, H. Yuan, H. Peng, J. Lim, A study on bone cement containing magnesium potassium phosphate for bone repair, Cogent Biol. 4 (2018).
[16] Y. Yu, C. Xu, H. Dai, Preparation and characterization of a degradable magnesium phosphate bone cement, Regen. Biomater. 3 (2016) 231–237.
[17] S. Yu, L. Liu, C. Xu, H. Dai, Magnesium phosphate based cement with improved setting, strength and cytocompatibility properties by adding $Ca(H_2PO_4)_2{\cdot}H_2O$ and citric acid, J. Mech. Behav. Biomed. Mater. 91 (2019) 229–236.
[18] B. Xu, B. Lothenbach, A. Leemann, F. Winnefeld, Reaction mechanism of magnesium potassium phosphate cement with high magnesium-to-phosphate ratio, Cem. Concr. Res. 108 (2018) 140–151.
[19] M. Le Rouzic, T. Chaussadent, L. Stefan, M. Saillio, On the influence of Mg/P ratio on the properties and durability of magnesium potassium phosphate cement pastes, Cem. Concr. Res. 96 (2017) 27–41.
[20] C.K. Chau, F. Qiao, Z. Li, Potentiometric study of the formation of magnesium potassium phosphate hexahydrate, J. Mater. Civ. Eng. 24 (2012) 586–591.
[21] H. Ma, B. Xu, J. Liu, H. Pei, Z. Li, Effects of water content, magnesia-to-phosphate molar ratio and age on pore structure, strength and permeability of magnesium potassium phosphate cement paste, Mater. Des. 64 (2014) 497–502.

[22] C. You, J. Qian, J. Qin, H. Wang, Q. Wang, Z. Ye, Effect of early hydration temperature on hydration product and strength development of magnesium phosphate cement (MPC), Cem. Concr. Res. 78 (2015) 179–189.
[23] B. Lothenbach, B. Xu, F. Winnefeld, Thermodynamic data for magnesium (potassium) phosphates, Appl. Geochem. 111 (2019) 104450.
[24] S. Zhang, H. Shi, S. Huang, P. Zhang, Dehydration characteristics of struvite-K pertaining to magnesium potassium phosphate cement system in non-isothermal condition, J. Therm. Anal. Calorim. 111 (2012) 35–40.
[25] L.J. Gardner, V. Lejeune, C.L. Corkhill, S.A. Bernal, J.L. Provis, M.C. Stennett, N. C. Hyatt, Evolution of phase assemblage of blended magnesium potassium phosphate cement binders at 200° and 1000°C, Adv. Appl. Ceram. 114 (2015) 386–392.
[26] X. Gao, A. Zhang, S. Li, B. Sun, L. Zhang, The resistance to high temperature of magnesia phosphate cement paste containing wollastonite, Mater. Struct. 49 (2016) 3423–3434.
[27] Y. Li, T. Shi, B. Chen, Y. Li, Performance of magnesium phosphate cement at elevated temperatures, Constr. Build. Mater. 91 (2015) 126–132.
[28] F. Di Lorenzo, C. Ruiz-Agudo, A. Ibañez-Velasco, R. Gil-San Millán, J.A.R. Navarro, E. Ruiz-Agudo, C. Rodriguez-Navarro, The carbonation of wollastonite: a model reaction to test natural and biomimetic catalysts for enhanced CO_2 sequestration, Materials 8 (2018) 209.
[29] P. Laniesse, C. Cau Dit Coumes, A. Poulesquen, A. Bourchy, A. Mesbah, G. Le Saout, P. Gaveau, Setting and hardening process of a wollastonite-based brushite cement, Cem. Concr. Res. 106 (2018) 65–76.
[30] H.A. Colorado, Z. Wang, J.-M. Yang, Inorganic phosphate cement fabricated with wollastonite, barium titanate, and phosphoric acid, Cem. Concr. Compos. 62 (2015) 13–21.
[31] W. Ashraf, J. Olek, N. Tian, Multiscale characterization of carbonated wollastonite paste and application of homogenization schemes to predict its effective elastic modulus, Cem. Concr. Compos. 72 (2016) 284–298.
[32] B. Lothenbach, F. Winnefeld, Thermodynamic modelling of the hydration of Portland cement, Cem. Concr. Res. 36 (2006) 209–226.
[33] B. Lothenbach, T. Matschei, G. Möschner, F.P. Glasser, Thermodynamic modelling of the effect of temperature on the hydration and porosity of Portland cement, Cem. Concr. Res. 38 (2008) 1–18.
[34] R.J. Myers, B. Lothenbach, S.A. Bernal, J.L. Provis, Thermodynamic modelling of alkali-activated slag cements, Appl. Geochem. 61 (2015) 233–247.
[35] F. Winnefeld, B. Lothenbach, Hydration of calcium sulfoaluminate cements — experimental findings and thermodynamic modelling, Cem. Concr. Res. 40 (2010) 1239–1247.
[36] R. Snellings, J. Chwast, Ö. Cizer, N. De Belie, Y. Dhandapani, P. Durdzinski, J. Elsen, J. Haufe, D. Hooton, C. Patapy, M. Santhanam, K. Scrivener, D. Snoeck, L. Steger, S. Tongbo, A. Vollpracht, F. Winnefeld, B. Lothenbach, Report of TC 238-SCM: hydration stoppage methods for phase assemblage studies of blended cements—results of a round robin test, Mater. Struct. 51 (2018) 111.
[37] R. Snellings, J. Chwast, Ö. Cizer, N. De Belie, Y. Dhandapani, P. Durdzinski, J. Elsen, J. Haufe, D. Hooton, C. Patapy, M. Santhanam, K. Scrivener, D. Snoeck, L. Steger, S. Tongbo, A. Vollpracht, F. Winnefeld, B. Lothenbach, RILEM TC-238 SCM recommendation on hydration stoppage by solvent exchange for the study of hydrate assemblages, Mater. Struct. 51 (2018) 172.
[38] T. Wagner, D.A. Kulik, F.F. Hingerl, S.V. Dmytrieva, GEM-Selektor geochemical modelling package: TSolMod library and data interface for multicomponent phase models, Can. Mineral. 50 (2012) 1173–1195.
[39] D.A. Kulik, T. Wagner, S.V. Dmytrieva, G. Kosakowski, F.F. Hingerl, K.V. Chudnenko, U.R. Berner, GEM-Selektor geochemical modeling package: revised algorithm and GEMS3K numerical kernel for coupled simulation codes, 17 (2013) 1–24.
[40] T. Thoenen, W. Hummel, U. Berner, E. Curti, The PSI/Nagra Chemical Thermodynamic Database 12/07, PSI Report 14-04, Villigen PSI, Switzerland, 2014.
[41] B. Lothenbach, D.A. Kulik, T. Matschei, M. Balonis, L. Baquerizo, B. Dilnesa, G. D. Miron, R.J. Myers, Cemdata18: a chemical thermodynamic database for hydrated Portland cements and alkali-activated materials, Cem. Concr. Res. 115 (2019) 472–506.
[42] E. Bernard, B. Lothenbach, C. Cau Dit Coumes, C. Chlique, A. Dauzères, I. Pochard, Magnesium and calcium silicate hydrates, part I: investigation of the possible magnesium incorporation in calcium silicate hydrate (C-S-H) and of the calcium in magnesium silicate hydrate (M-S-H), Appl. Geochem. 89 (2018) 229–242.
[43] W.F. Jaynes, P.A. Moore, D.M. Miller, Solubility and ion activity products of calcium phosphate minerals, J. Environ. Qual. 28 (1999) 530–536.
[44] Q. Liu, Z. Chen, H. Pan, B.W. Darvell, The effect of excess phosphate on the solubility of hydroxyapatite, Ceram. Int. 40 (2014) 2751–2761.
[45] R.A. Robie, B.S. Hemingway, Thermodynamic properties of minerals and related substances at 298.15 K and 1 bar (10^5 pascals) pressure and at higher temperatures, Bulletin, 1995.
[46] D.A. Kulik, Minimising Uncertainty Induced by Temperature Extrapolations of Thermodynamic Data: A Pragmatic View on the Integration of Thermodynamic Databases Into Geochemical Computer Codes, Organisation for Economic Co-Operation and Development - Nuclear Energy Agency, Nuclear Energy Agency of the OECD (NEA), 2002.
[47] G.M. Anderson, D.A. Crerar, Thermodynamics in Geochemistry: The Equilibrium Model, Oxford University Press, Oxford, 1993.
[48] D. Quenard, M. Carcasses, Gas permeability of concrete: definition of a preconditioning procedure for measurements and crossover trials. , in: M.A. Lacasse, D.J. Vanier (Eds.) Durability of building materials and components 8, Institue for Research in Construction, Ottawa, ON, KIA 0R6, Canada 1999, pp. 236–245.
[49] L.J. Parrott, Moisture conditioning and transport properties of concrete test specimens, Mater. Struct. 27 (1994) 460.
[50] S.H. Lee, B.H. Yoo, S.K. Kim, S.J. Lim, J.Y. Kim, T.H. Kim, Enhancement of struvite purity by re-dissolution of calcium ions in synthetic wastewaters, J. Hazard. Mater. 261 (2013) 29–37.
[51] H. Yan, K. Shih, Effects of calcium and ferric ions on struvite precipitation: a new assessment based on quantitative X-ray diffraction analysis, Water Res. 95 (2016) 310–318.
[52] B. Lothenbach, P. Durdziński, K.D. Weerdt, Thermogravimetric analysis, in: K. Scrivener, R. Snellings, B. Lothenbach (Eds), A practical guide to microstructural analysis of cementitious materials, pp. 177–212, Taylor & Francis Group, 2016.
[53] T. Isobe, S. Nakamura, R. Nemoto, M. Senna, H. Sfihi, Solid-state double nuclear magnetic resonance study of the local structure of calcium phosphate nanoparticles synthesized by a wet-mechanochemical reaction, J. Phys. Chem. B 106 (2002) 5169–5176.
[54] F. Pourpoint, C. Gervais, L. Bonhomme-Coury, T. Azaïs, C. Coelho, F. Mauri, B. Alonso, F. Babonneau, C. Bonhomme, Calcium phosphates and hydroxyapatite: solid-state NMR experiments and first-principles calculations, Appl. Magn. Reson. 32 (2007) 435–457.
[55] E. Bernard, B. Lothenbach, F. Le Goff, I. Pochard, A. Dauzères, Effect of magnesium on calcium silicate hydrate (C-S-H), Cem. Concr. Res. 97 (2017) 61–72.
[56] E. Bernard, B. Lothenbach, C. Chlique, M. Wyrzykowski, A. Dauzères, I. Pochard, C. Cau-Dit-Coumes, Characterization of magnesium silicate hydrate (M-S-H), Cem. Concr. Res. 116 (2019) 309–330.
[57] H. Ma, B. Xu, Z. Li, Magnesium potassium phosphate cement paste: degree of reaction, porosity and pore structure, Cem. Concr. Res. 65 (2014) 96–104.
[58] W. Kunther, Z. Dai, J. Skibsted, Thermodynamic modeling of hydrated white Portland cement–metakaolin–limestone blends utilizing hydration kinetics from ^{29}Si MAS NMR spectroscopy, Cem. Concr. Res. 86 (2016) 29–41.
[59] L.J. Gardner, S.A. Bernal, S.A. Walling, C.L. Corkhill, J.L. Provis, N.C. Hyatt, Characterisation of magnesium potassium phosphate cements blended with fly ash and ground granulated blast furnace slag, Cem. Concr. Res. 74 (2015) 78–87.
[60] J. Skibsted, High-resolution solid-state nuclear magnetic resonance spectroscopy of portland cement-based systems, in: K. Scrivener, R. Snellings, B. Lothenbach (Eds), A practical guide to microstructural analysis of cementitious materials, pp. 213–286., Taylor & Francis Group, 2016.
[61] M.R. Hansen, H.J. Jakobsen, J. Skibsted, ^{29}Si chemical shift anisotropies in calcium silicates from high-field ^{29}Si MAS NMR spectroscopy, Inorg. Chem. 42 (2003) 2368–2377.
[62] S.N. Scrimgeour, J.A. Chudek, C.H. Lloyd, The determination of phosphorus containing compounds in dental casting investment products by ^{31}P solid-state MAS-NMR spectroscopy, Dent. Mater. 23 (2007) 415–424.
[63] J.F. Stebbins, W.R. Panero, J.R. Smyth, D.J. Frost, Forsterite, wadsleyite, and ringwoodite (Mg_2SiO_4): ^{29}Si NMR constraints on structural disorder and effects of paramagnetic impurity ions, Am. Mineral. 94 (2009) 626–629.
[64] D.R. Spearing, J.F. Stebbins, The ^{29}Si NMR shielding tensor in low quartz, Am. Mineral. 74 (1989) 956–959.
[65] I. Klur, B. Pollet, J. Virlet, A. Nonat, C-S-H structure evolution with calcium content by multinuclear NMR, in: P. Colombet, H. Zanni, A.R. Grimmer, P. Sozzani (Eds.), Nuclear Magnetic Resonance Spectroscopy of Cement-Based Materials, Springer Berlin Heidelberg, 1998, pp. 119–141.
[66] B. Lothenbach, D. Nied, E. L'Hôpital, G. Achiedo, A. Dauzères, Magnesium and calcium silicate hydrates, Cem. Concr. Res. 77 (2015) 60–68.
[67] M.A. Aramendía, V. Borau, C. Jiménez, J.M. Marinas, F.J. Romero, J.R. Ruiz, XRD and solid-state NMR study of magnesium oxide–magnesium orthophosphate systems, J Solid State Chem, 135 (1998) 96–102.
[68] Y. Wu, J.L. Ackerman, E.S. Strawich, C. Rey, H.M. Kim, M.J. Glimcher, Phosphate ions in bone: identification of a calcium-organic phosphate complex by ^{31}P solid-state NMR spectroscopy at early stages of mineralization, Calcif. Tissue Int. 72 (2003) 610–626.
[69] Y.H. Tseng, J. Zhan, K.S.K. Lin, C.Y. Mou, J.C.C. Chan, High resolution ^{31}P NMR study of octacalcium phosphate, Solid State Nucl. Magn. Reson. 26 (2004) 99–104.